



Western Michigan University
ScholarWorks at WMU

Dissertations

Graduate College

6-2007

Some Applications of Gaussian Quadrature and Neural Network Modeling in Earth Flows and Other Slow-Moving Landslides in Cohesive Slope Materials

Rennie Bwalya Kaunda
Western Michigan University

Follow this and additional works at: <https://scholarworks.wmich.edu/dissertations>



Part of the Geology Commons

Recommended Citation

Kaunda, Rennie Bwalya, "Some Applications of Gaussian Quadrature and Neural Network Modeling in Earth Flows and Other Slow-Moving Landslides in Cohesive Slope Materials" (2007). *Dissertations*. 3444. <https://scholarworks.wmich.edu/dissertations/3444>

This Dissertation-Open Access is brought to you for free and open access by the Graduate College at ScholarWorks at WMU. It has been accepted for inclusion in Dissertations by an authorized administrator of ScholarWorks at WMU. For more information, please contact wmu-scholarworks@wmich.edu.



SOME APPLICATIONS OF GAUSSIAN QUADRATURE AND NEURAL
NETWORK MODELING IN EARTH FLOWS AND OTHER
SLOW-MOVING LANDSLIDES IN COHESIVE
SLOPE MATERIALS

by

Rennie Bwalya Kaunda

A Dissertation
Submitted to the
Faculty of The Graduate College
in partial fulfillment of the
requirements for the
Degree of Doctor of Philosophy
Department of Geosciences

Western Michigan University
Kalamazoo, Michigan
June 2007

Copyright by
Rennie Bwalya Kaunda
2007

ACKNOWLEDGMENTS

Special gratitude goes to my research advisor Dr. Ronald Chase for all his support and advice during my graduate student career. His unwavering labors on my behalf made it possible for me to brave the winters of Michigan in pursuit of a doctorate education.

I would also like to acknowledge my dissertation committee: Dr. Alan Kehew, Dr. William Sauck, Department of Geosciences, Western Michigan University, Dr. Karlis Kaugars, Department of Computer Sciences, Western Michigan University, and Dr. James Selegan, US Army Corps of Engineers-Detroit District. Also Dr. Jay Treiman from the Mathematics Department, Western Michigan University was helpful with the numerical analysis. My understanding of groundwater hydraulics was also broadened with the help of Dr. Duane Hampton, Department of Geosciences, Western Michigan University.

I wish to acknowledge funding from the Engineering Research and Development Center (ERDC), and the Detroit District, US Army Corps of Engineers. Western Michigan University generously provided both financial and logistical support. I am also grateful to the property owners in Allegan County, MI, Allegan County Road Commission and State of Michigan for granting access to the study site.

Finally, I wish to thank my very understanding family and friends for all their

Acknowledgments—continued

support, patience and unyielding faith that my prolonged stay in school would bear tangible fruit someday. My wife, Jami, ensured that I stayed sane and healthy by monitoring my meals and hours of sleep. My parents, Robert and Bertha, never gave up praying for me and my brothers and sisters kindly tolerated my absences from many family reunions.

Rennie Bwalya Kaunda

SOME APPLICATIONS OF GAUSSIAN QUADRATURE AND NEURAL
NETWORK MODELING IN EARTH FLOWS AND OTHER
SLOW-MOVING LANDSLIDES IN COHESIVE
SLOPE MATERIALS

Rennie Bwalya Kaunda, Ph.D.

Western Michigan University, 2007

Geometrical changes and progressive displacements in earth flows and other slow moving landslides triggered by climatic changes may be addressed by digital modeling. Gaussian quadrature, a numerical integration technique though fixed points, is employed to compute geometrical areas defined by stratigraphic (soil or rock layering) units, vertical pole projections and a slip surface, based on kinematic admissibility. An example from the Lake Michigan coast shows that the total internal geometrical area is found to be preserved during the course of the progressive deformation. Displacement monitoring of the slope shows that it became less stable over a period of eleven years due to progressive failure. The Gaussian quadrature technique allows representation and manipulation of geometrical models in a digital format amenable to the display of volumetric changes. Four different types of neural network models are also developed based on the back propagation algorithm for landslide problems in Michigan, England and the French Alps. The first Artificial

Neural Network model predicts slip surface positions based on measured surface displacements and soil types. The second neural network model predicts slope displacement rates from temperature and groundwater level data. The third model predicts ground water levels based on temperature data. The fourth model predicts displacements from precipitation records. The predicted slip surface positions using artificial neural networks closely match the measured positions of slip surfaces at all three sites. Also, the neural network models are able to predict ground water levels and displacements from climate data. The digital exactness of Gaussian quadrature and neural network modeling allows for applications that are in a usable, quantifiable format for engineers and other mitigation planners. This digital format can be applied to a wide variety of slope stability problems of concern.

TABLE OF CONTENTS

ACKNOWLEDGMENTS	ii
LIST OF TABLES	vii
LIST OF FIGURES.....	viii
CHAPTER	
I. INTRODUCTION	1
Organization of the Dissertation.....	1
Problem Statement	1
Study Objectives.....	4
Methods of Developing Digital Models.....	5
Using Gaussian Quadrature to Constrain Deformation Models.....	5
Artificial Neural Networks (ANN) Modeling.....	6
Testing the Models	9
Usefulness of the Modeling Methods.....	11
II. USING GAUSSIAN QUADRATURE IN SLOPE STABILITY MODELING STUDIES	13
Introduction	13
Geometric Modeling of the Subsurface.....	14
The Process of Cross-Section Balancing.....	17
The Use of Gaussian Quadrature.....	20

Table of Contents—continued

CHAPTER

Using Gaussian Quadrature to Balance a Cross Section	22
Results of the Gaussian Quadrature Application to Line 2	27
Application to the Process of Slope Stability Analysis	28
Conclusions	30
III. SOME APPLICATIONS OF NEURAL NETWORK MODELING IN ACTIVE SLOPE PROBLEMS	32
Introduction	32
Artificial Neural Networks (ANN).....	34
Predicting Slip Surface Locations from Displacements with Artificial Neural Networks.....	36
The Problem of Slip Surface Location.....	36
Data Acquisition	37
Artificial Neural Network Training and Testing.....	39
Results of the Artificial Neural Network Testing for Miami Park South.....	44
Sensitivity Analysis for the Slip Surface Prediction	46
Example 1: La Mure Landslide, French Alps.....	48
Description.....	48
Artificial Neural Network Model Set Up for the La Mure Landslide	50
Example 2: Mam Tor Landslide, Derbyshire, England.....	52
Description.....	52
Artificial Neural Network Model Set Up for the Mam Tor Landslide.....	53

Table of Contents—continued

CHAPTER

Predicting Displacements from Meteorological and Groundwater Data using Artificial Neural Networks	55
Using Groundwater Potentiometric Surface Elevations and Air Temperatures to Predict Displacements	55
Using Air Temperatures to Predict Groundwater Potentiometric Surface Elevations	58
Example 3: La Mure Landslide Displacements.....	59
Description.....	59
Artificial Neural Network Model Set Up for La Mure Displacements.....	60
Summary and Conclusions.....	63

APPENDICES

A. Gaussian Quadrature.....	65
B. Back Propagation Algorithm	70

BIBLIOGRAPHY	78
--------------------	----

LIST OF TABLES

1. Pre-selected points of integration and their associated weights for the Gauss-Legendre rule	21
2. Gaussian Quadrature Spreadsheet for the first stratigraphic layer of lacustrine clay before and after deformation.....	25
3. A comparison of initial and final layer areas obtained from Gaussian quadrature spreadsheets in units squared	28
4. Effective stress geotechnical parameters used for the slope stability analysis.....	29
5. Sample training file from MPS	41
6. Summary statistics for neural network training and testing for slip surface depth prediction.....	46
7. Sensitivity analysis for slip surface depth prediction.....	47
8. Summary of statistical modeling results for the neural network displacement rates prediction at various time lags.....	57
9. Summary of statistical modeling results for the neural network ground water elevation prediction at various time lags.....	58
10. Summary of neural network displacement modeling results of La Mure Landslide compared with displacements measured by Recorder L1 and L3	60

LIST OF FIGURES

1. One of the pole-and-cable displacement monitoring lines installed on a Lake Michigan slump system.....	15
2. Stratigraphic displacement of a cross section in the Miami Park South slump zone showing the changing internal geometry	16
3. Cross section balancing illustration in which all original line lengths and angles are preserved	18
4. Map of study area showing positions of five pole-and-cable monitoring systems	20
5. Layer boundaries	23
6. Digitization of the four stratigraphic layers	27
7. Limit equilibrium analysis results of slope using geometric field conditions: A) June 10, 1996; B) June 10, 2003.....	30
8. Artificial Neural Network layered arrangement of input, hidden and output nodes in a Multi Layer Perceptron (MLP) or feed forward architecture.....	35
9. Location of the Miami Park South site	37
10. The pole-and-cable slope displacement monitoring system	38
11. Slope geometric evolution	40
12. Neural network training and test results	43
13. Model fit showing predicted slip surface depths versus true depths for test data	45
14. The La Mure Landslide in the French Alps	49
15. Slip surface predictions for La Mure	51
16. Critical search for slip surface using limit equilibrium analysis and Bishop's method for the four slope profiles shown in Figure 14.....	52

List of Figures—continued

17. Location and aerial map of the Mam Tor Landslide in Derbyshire, England	53
18. Slip surface prediction results for Mam Tor	54
19. Time series curves showing displacement rates, air temperature and groundwater elevation from well number 11 at the Miami Park South site (Figure 9).....	56
20. Correlation between displacements predicted by the Artificial Neural Network modeling and displacements measured from the field by recorders: A) L1 and B) L3 in Figure 13 for the La Mure Landslide.....	61
21. Cumulative displacements and precipitation over time for the La Mure Landslide	62

CHAPTER I

INTRODUCTION

Organization of the Dissertation

This dissertation is divided into three parts: General Introduction, Paper 1 and Paper 2. This General Introduction consists of the definition and context of the problem, and the study objectives. Paper 1 discusses the application of Gaussian quadrature in geometric modeling of active landslides. Paper 2 discusses three different categories of Artificial Neural Network modeling: predicting slip surface positions in an active landslide based on measured displacements, predicting groundwater potentiometric surface elevations in an active landslide based on climate data, and predicting displacements from climate data.

Problem Statement

The destruction from landslides remains a serious worldwide concern because it threatens houses, commercial buildings, roads and other infrastructure located along coastal cliffs or hill slopes (Hampton et al., 2004). Property losses may reduce local tax revenues, affect federal disaster relief and insurance, and cause financial losses to the tourism industry. Soil or rock displacement may also destroy lives, create conditions for point source pollution, and disrupt the beauty of the landscape. Landslides are becoming an increasing socio-economic concern as world population increases causing human development to expand into unstable hillslope areas (Schuster, 1996). Hampton et al. (2004) have highlighted some of the major

challenges affecting the problem of coastal landslides, which may also be extrapolated to non-coastal landslides. These include understanding the fundamental processes and factors involved, documenting and quantifying the spatial and temporal variations of retreat rates and providing data in usable format to coastal engineers, planners, managers, and the general public.

Landslides can be triggered by mechanisms such as unusual precipitation, water table rises or drops, earthquakes, and volcanic eruptions, all of which affect the slope material properties. Although these triggering mechanisms are all important, the role of hydraulics is especially significant because it occurs in various forms. For example, shallow landslides in soils and weathered rock may be generated in steep slopes during the more intense parts of a storm, when the intensity and duration of precipitation are above a certain threshold (Wieczorek, 1996). The rapid infiltration of rain, may cause soil saturation and a temporary rise in pore pressure which decreases the effective strength of saturated slope materials and thus trigger landslides (Sidle, 1984, Wilson and Dietrich 1987, Reid et al., 1988 Wilson, 1989, Johnson and Sitar, 1990, Simon et al., 1990). The process of snow melting could also provide a continuous supply of moisture over a longer time period compared with the usual duration of infiltration from rain (Horton, 1938). Snowmelt may recharge shallow fractured bedrock and raise pore-water pressures beneath shallow soils, thus triggering landslides (Mathewson et al., 1990). Pore pressure increase can also occur during rising groundwater levels in hill slopes following periods of prolonged above-normal precipitation or during the raising of water levels in lakes and reservoirs adjacent to the slope (Wieczorek, 1996). Rapid drawdown can also trigger landslides when the water level in a reservoir or unstable slope is dropped suddenly (Lambe and Whitman, 1969). There is critical need, therefore, for good digital models capable of

evaluating potential for landslide displacements based on triggering mechanisms related to climate and/or hydraulics.

Slope stability problems can build in a progressive manner (Chowdhury, 1978; Suemine, 1983; Kamai, 1998; Cooper et al., 1998; Petley et al., 2005). Progressive failure refers to the idea first introduced by Terzaghi and others (1948) that a natural slope can fail or collapse at an average shear stress less than the actual peak shear strength of the slope material. As the slope is being loaded non-uniformly by incremental shear displacements, the shear strength of the slope material falls below the peak value. Progressive failure can occur in special types of landslides known as earthflows/slumps (Varnes, 1978). In slow moving landslides, movements can be reactivated along old slip surfaces. Therefore any method that can trace/assess the movements or predict new or old slip surface positions can be extremely useful for evaluating land sliding. The reason it is difficult to study and understand progressive ground failure is because testing stress-strain relations directly in the field may not produce accurate results. Also, laboratory tests on slope-material do not necessarily reflect field conditions. For example, studies have shown that a change in the rate at which a brittle soil is loaded can change its shear strength significantly and affect slope stability (Srbulov, 1999). There is a critical need for accurate geometric models capable of evaluating land sliding via progressive failure. It is imperative to have a thorough understanding of slip surface geometry and location or the internal geometry of the sliding blocks, key components to understanding slope displacement kinetics and the future of the slope (Nieuwenhuis, 1991, Chase et al., 2001b).

Traditionally the search for a critical slip surface for slope displacements has been assessed by limit equilibrium analysis using methods of slices, such as Bishop's method, Spencer's method and Janbu's method depending on problem type (Duncan,

1996a). Because most of these methods rely on assumptions related to positioning of slice forces to work, researchers have applied alternatives in the pursuit of methods superior to limit equilibrium analysis. These alternatives include linear programming, Monte Carlo simulation techniques, and finite element modeling techniques (Kim and Lee, 1997, Griffiths and Lane, 1999, Chen, 2004, and Yang et al., 2004). Because these techniques require geotechnical input parameters such as an accurate understanding of the stress-strain behavior of the slope materials (Duncan, 1996b), they are often limited by the available ground truth data. Additionally, in these techniques, a fundamental assumption is made that the field system being modeled obeys the stress-strain behavior observed in the laboratory. However this may not always be true, as in the case of progressively failing landslides discussed above.

Study Objectives

The foregoing discussion clearly demonstrates the significance of stress/strain and deformation history, layer geometry, ground water elevations, and climatic parameters such as precipitation and air temperature in analyzing slope stability problems. Therefore qualitative and quantitative inclusion of these parameters in modeling using real field data can increase understanding of their role in slope displacements. The objective of this research is to develop and apply field data-based modeling techniques useful in assessing progressive landslide behavior. The goals of this work are as follows:

1. Develop digital models that are as free as possible of human interpretation for:
 - establishing the depth and shape of critical slip surfaces at the base of landslide blocks.

- establishing the internal displacements that landslide blocks might experience when adjusting to their new geometries above the critical surfaces.
 - establishing relationships among climate, hydraulics, and displacements.
2. Demonstrate that the digital models thus developed compare favorably with the field conditions where appropriate data are available.
 3. Demonstrate that the models are useful for a variety of slope stability problems and solutions, where field and/or laboratory data are incomplete

Methods of Developing Digital Models

Using Gaussian Quadrature to Constrain Deformation Models

For many years structural geologists have applied principles of cross section balancing to geologic-scale, regionally-deformed terrain to establish displaced geometry (e.g. Dahlstrom, 1969, Woodward et al., 1985, Suppe and Mededeff, 1990). These balancing methods are adaptable to multiple applications (e.g. Erslev, 1991; Hardy and Ford, 1997; Waltham, 1992; Allmendinger, 1998 and Finch et al, 2003). Chase and others (2001a, 2007a) have applied balancing concepts to slope stability problems for characterizing slope evolution during progressive failure. The goal is to determine internal deformation patterns and depths and geometries of slip surfaces in

unstable bluffs along the southeastern shoreline of Lake Michigan. The fundamental concept is that each cross section is defined by pin lines at both ends, and the total length of the stratigraphic geometry within each section is preserved. Therefore, after deformation has occurred, neither line lengths nor cross-sectional areas of stratigraphic units are allowed to change. Disturbed layers can be restored to their original positions without introducing or eliminating areas within stratigraphic profiles. To apply cross section balancing to unconsolidated materials, near-vertical grid lines initially divide the cross section area into a group of polygonal segments. There should be sufficient rigidity of the material such that volume changes during segment deformation are minimal.

The cross-section balancing method is highly intuitive and extremely time consuming when conducted by freehand or when dealing with multiple sliding blocks (Chase et al., 2007a). There is, therefore, need for an efficient technique to digitally check the accuracy of the balancing, then identify and quantify any corrections required, hence the application of Gaussian quadrature discussed in Paper 1.

Artificial Neural Networks (ANN) Modeling

Artificial Neural Networks (ANN) are a system of interconnected, computational nodes or processing elements fashioned after biological neurons of the nervous system. All ANN have three things in common: nodes, connection weights and layers containing the nodes. A major advantage of ANN over other models, such as purely mathematical ones, is their ability to learn complex relationships among data sets. Once this knowledge is acquired, they may then be applied in instances of limited data. In other words, they can learn and generalize. Artificial Neural Networks are described by their architecture and their learning algorithm. In this

study, a feed-forward architecture was used, implying layers of computational nodes are connected to other layers in one direction, from the input to the output layer. The learning algorithm that was used is the back-propagation algorithm, because it is very robust and easy to implement. The back propagation algorithm was first invented by Werbos (1974). Back propagation was later inadvertently reinvented by Parker, (1985), and presented to wide readership by Rumelhart and McClelland(1986).

Artificial Neural Networks have found a wide application in the geosciences including geotechnical work. For example, Ellis et al. (1995) modeled the stress-strain behavior of sands using Artificial Neural Networks. Undrained triaxial compression tests were conducted on eight different sands to generate data for neural network training and testing. The neural network was developed sequentially with a feed back capability. The study demonstrated that a general Artificial Neural Network could be developed that accounted for particle size distribution and stress history effects. Ghaboussi and Sidarta (1998) applied adaptive neural network modeling to drained compression test results for Sacramento River sand. The neural net was trained directly with material test results, and used in the analysis of boundary value problems in constitutive modeling. The neural network was successfully applied in modeling drained and undrained sand stresses from triaxial tests. Zhu et al. (1998) applied ANN to the prediction of shear behavior in a fine-grained residual soil and dune sand. The neural network was trained using strain-controlled undrained tests and stress-controlled drained tests performed on a residual Hawaiian volcanic soil. The neural net had feedback connections from the hidden layer to the input layer. Agreements between the measured data and the modeling results were observed in both stress-strain behavior and volumetric-change characteristics of the soil. Juang et al. (2001) utilized ANN for subsurface site characterization using cone penetrometer

(CPT) data in sand. Cone tip resistances were predicted in 1 dimension (depth), 2-dimensions (x, y-coordinates in space) and 3 –dimensions (x, y and z coordinates) at various spreads of the cone penetrometer. The approach was found to be effective in generalizing soil properties based on limited in-situ CPT tests. Habibagahi and Bamdad (2003) applied ANN to predict deviatoric stress, volume and suction change from triaxial test results. The input parameters consisted of water content, dry density, degree of saturation, soil suction, axial strain and deviatoric stress, with a feedback (loop) mechanism. When the neural network simulations were compared with triaxial test results, the comparisons indicated good predictions of the mechanical behavior (stress-strain, suction change, and volume change) of the unsaturated soil.

Cao (2002) applied detailed neural network modeling to slope stability analysis to predict factors of safety. The network was a two-layer recurrent neural network with a sigmoid hidden layer and linear output layer. The input parameters included slope height, slope inclination, water level height, tension crack position height, soil unit weight, soil cohesion, soil friction angle, layer thickness, and pore water pressure to overburden pressure ratio per layer. The output layer had only one neuron, namely the factor of safety. The predictions made by the neural net were comparable to results obtained from finite element modeling.

In this study four types of ANN models are developed based on the back propagation algorithm, with the goal of addressing some problems associated with slow moving landslides:

- Prediction of the positions of slip surfaces in an active landslide in Michigan based on measured surface displacements and soil types. In this model type the number of input parameters is systematically varied in a sensitivity

analysis to determine the significance of each input. This was conducted to compensate for the problem of data unavailability typical in practical applications.

- Prediction of slope displacement rates from temperature and groundwater level data.
- Prediction of ground water levels based on temperature data.
- Prediction of displacements from precipitation records.

Testing the Models

The models developed in this study are tested using actual field data. Gaussian quadrature modeling was tested using drill and displacement records from Miami Park South, Michigan. The site is located along the southeastern shoreline bluffs of Lake Michigan in Allegan County, about five miles north of South Haven, Michigan. This site, which is known to be unstable, has well documented movement history and geology. The average rate of recession is 1.3 ft (0.39 m) per year. These bluffs have an average height of about 80 ft (24 m), and a slope angle of about 34 degrees. At the beach level is a gray, massive, clay-rich diamicton that is over-consolidated and locally jointed. Above this unit are inter-layered sand and laminated clay. The sand is generally tan colored and layers range in thickness from 1 cm to 10 m or more. It is fine-grained, well-sorted and rounded, and contains cross-beds and ripple marks. The laminated clay is brown to gray with alternating light and dark laminations about 1-3 mm thick. Layers range from 1 cm to 3 m thick. This clay is normally consolidated and highly plastic with low yield strength. Overlying these inter-layered units, is a sandy to silty diamicton. It is brown to gray in color, normally

consolidated and highly jointed.

The Artificial Neural Network modeling was tested on field data from two other sites in addition to Miami Park South. The first site is a landslide problem in the French Alps. The site, located near Grenoble, was first investigated by Van Genuchten and Nieuwenhuis (1990), and later in greater detail by Nieuwenhuis, (1991). The landslide, developed in varved clays, has movements known to be greater than one meter per year. The dimensions of the study area were about 500 m long and 125 m high. Soils consist of mostly over-consolidated silty clays with residual shear strengths. The displacements occur along existing slip surfaces and movements are seasonal driven by excessive precipitation or snow melt. The hydrology of the area is complex due to the presence of scarps and fissures.

The second site is the Mam Tor landslide in Derbyshire England. The Mam Tor landslide has been studied by Skempton et al. (1989) and more recently by Rutter et al. (2003). The landslide has a well documented movement history and geology. The landslide exhibits episodic and creep movements that led to the collapse of the eastern section and the formation of an 80 m high scarp. The dimensions of the slipped mass are about 750 m long and 500 m wide. The geology consists mostly of mudstone overlying sandstone. The average displacement rate is 10 cm per year, with the central region moving faster at 50 cm per year. Displacements have also been known to correlate with annual variations in rainfall above a critical threshold level. Stress/strain relationships are highly nonlinear with significant shearing strain occurring at very low levels of shearing stress.

The Gaussian quadrature model tested using the Miami Park South site produced results similar to expected values. The prediction of slip surface positions using Artificial Neural Networks closely matched measured positions at all three

sites, in spite of some scatter. The neural networks were also able to predict ground water levels and displacements from climate data.

Usefulness of the Modeling Methods

These techniques, though developed with real field data, are not meant to be the basis of slope engineering decisions which could potentially lead to the loss of life. They are meant to provide a foundation on which further detailed geotechnical investigations may be conducted. The manner in which the Gaussian quadrature and Artificial Neural Network models discussed here might be used for future geotechnical studies are listed below.

- 1) By virtue of being digital, both methods provide a usable, quantifiable format to engineers and other mitigation planners who can readily analyze or manipulate them mathematically based on the specific slope stability problem of concern.
- 2) The Gaussian quadrature approach can be used to check the consistency of the internal geometry of a slope or landslide undergoing gradual structural deformation in order to assess slope stability more reliably.
- 3) The Gaussian quadrature technique can be used to measure the degree of erosion a particular slope or landslide has been subjected to based on computed mass volumes.
- 4) The Gaussian quadrature technique can be used to compute the required correction required for the cross section balancing.

- 5) The Artificial Neural Network model may be useful when a factor of safety needs to be calculated for a slope whose critical failure surface location or geometry is not known. This neural network may also be used when planning placement of instrumentation such as piezometers, dewatering wells or other infrastructure.
- 6) All of the neural network models discussed could be used as a basis to develop a warning system for predicting slope displacement, dependent on climate and groundwater elevation observations.
- 7) The Artificial Neural Networks developed using the parameters discussed--soil types ground translations, ground elevation change, precipitation, air temperature--could be applied to other landslide problems and have these parameters experimented with, using sensitivity analysis, to determine which factors are significant for those specific sites.

CHAPTER II

USING GAUSSIAN QUADRATURE IN SLOPE STABILITY MODELING STUDIES

Introduction

The phenomenon of gradual movement in landslides creates a special challenge to the geology and engineering community because their geometric character can change over time (Chowdhury, 1978; Suemine, 1983; Kamai, 1997; Petley et al., 2005). Geometric and mathematical models can thus be critical tools to model their progressive failure. This is because they can help locate slip surfaces and give a realistic picture of the deformed internal geometry, which is especially valuable in slope stability modeling for multiple soil layers. It is imperative however, that such models are accurate and validated by field data. In the above types of hazards, geometric models showing the progression of the landslides over time can serve as important tools to determine or predict the evolution of a given slope. For example, Chase et al. (2001a, 2007a) describe a geometric model that has been successfully used to assess the internal deformation history of slowly moving slumps along the Lake Michigan coast using cross-section balancing techniques, described in the following sections. The model, based on slope displacement field data measured from the surface, is mostly intuitive. In this study Gaussian quadrature is used to evaluate the accuracy of this geometric construction model. The evaluation is done by computing and comparing internal geometrical areas determined by the model for the initial and final state of the slope after a period of progressive deformation. This procedure improves the accuracy of cross section constructions by producing a

mathematical-based model that is developed from field data and one that may be represented digitally. The validated geometric result can be put into a limit equilibrium program to assess the evolution and stability of the slope quantitatively.

Geometric Modeling of the Subsurface

Chase and others (2001a, 2007a) developed a geometric model useful for site characterization of the subsurface of a displaced slope. Surface displacements are measured by a pole-and-cable monitoring system. The system consists of eight-foot (2.5 m) fence poles vertically driven about five feet (1.5 m) into the ground and placed down the slope face in parallel rows, as shown in Figure 1. A steel cable marked with colored plastic tape at 1.5 inch (3.8 cm) intervals runs from the crest of the slope to the toe and is strung through each pole. Tri-weekly surveys of each row of poles consist of the measurement of distance between poles, cable height above ground at each pole, cable sag angles between poles, and pole inclination angles in both the strike and dip directions of the slope. By projecting measured surface translations and rotations into the subsurface, positions of slip (or shear) planes and displaced strata can be modeled with the aid of cross section balancing techniques. For example, Figure 2 shows the initial condition of a slope profile and progressive changes after deformation for a Lake Michigan coastal slump (Chase et al., 2007b). As the section deforms, its profile can be re-balanced periodically to display its changing internal geometry. The production of balanced cross sections is not restricted to only the pole and cable system. Any survey method that expresses

geometries at depth, such as inclinometer profiles, drill hole stratigraphy and extensometer records can produce balanced cross sections.



Figure 1. One of the pole-and-cable displacement monitoring lines installed on a Lake Michigan slump system. Each line is surveyed individually by measuring the distance between poles, cable height above ground at each pole, cable sag angles between poles, and pole inclination angles in both the strike and dip direction of the slope.

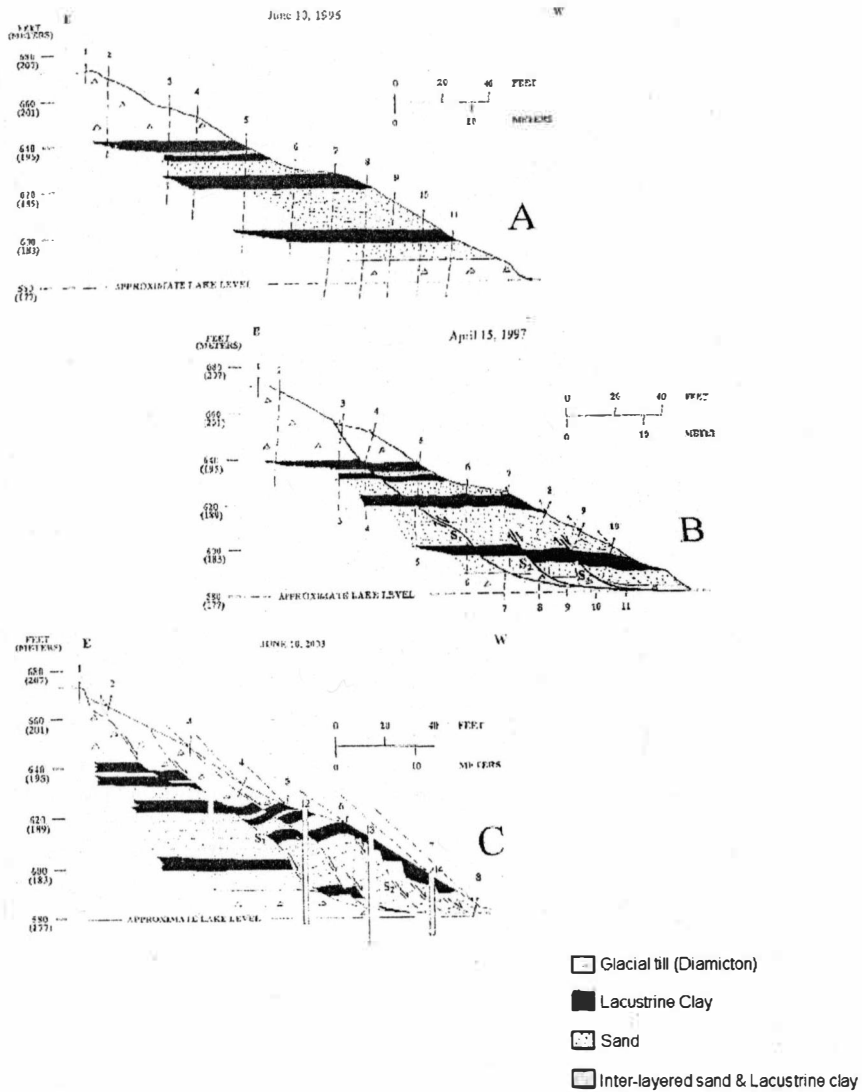


Figure 2. Stratigraphic displacement of a cross section in the Miami Park South slump zone showing the changing internal geometry. The profiles are constructed from repeated surveys and the geometric cross-section balancing. The displacements show: (A) initial conditions with horizontal strata and no slip surfaces; (B) one deep slip surface and two developing slip surfaces resulting in three fault blocks; and (C) final deformed state after seven years of progressive deformation (Chase et al., 2007a).

Source: Chase, R.B., Kehew, A.E., Glynn, M.E., and Selegean, J.P., 2007, Modeling debris slide geometry with balanced cross-sections: a rigorous field test: *Environmental & Engineering Geoscience*, 13(1), 193-203
Used with permission of Ronald B. Chase, Author, 5-14-07

The Process of Cross-Section Balancing

A cross section is said to be balanced if its geometry can be restored to its undeformed ideal state without violating kinematic admissibility (Dahlstrom, 1969, Woodward et al., 1985). Details of the adaptation of cross section balancing techniques to landslide studies can be found in Chase et al. (2001B, 2007A).

Given an initially undeformed segment of slope profile as represented by Figure 3A, changing ground surface conditions due to slip at depth will be reflected by pole translations and rotations. To balance the cross section the underlying area in the subsurface is divided into a series of horizontal parallel lines. Such lines are based on either stratigraphic contacts or arbitrary references. Additionally, the poles serve as reference “pin” lines which may be projected downward into the profile to generate a series of polygonal cells with defined initial shapes and areas. During progressive stages of landslide evolution, the positions and shapes of these cells will change (Figures 3B-3D) as reflected by pole rotations and translations. However, cell areas, corner angles, and line lengths must be preserved at each stage of the deformation. This is achieved by introducing folds and/or slip surfaces through each cell that can collectively pass through all cells in the section without violating the length/angle rule. For example, a normal slip is introduced in Figure 3B, fault propagation slip in Figure 3C and reverse slip in Figure 3D while preserving cell areas, corner angles and line lengths. Observed surface scarps or ground warps may be used to position slip

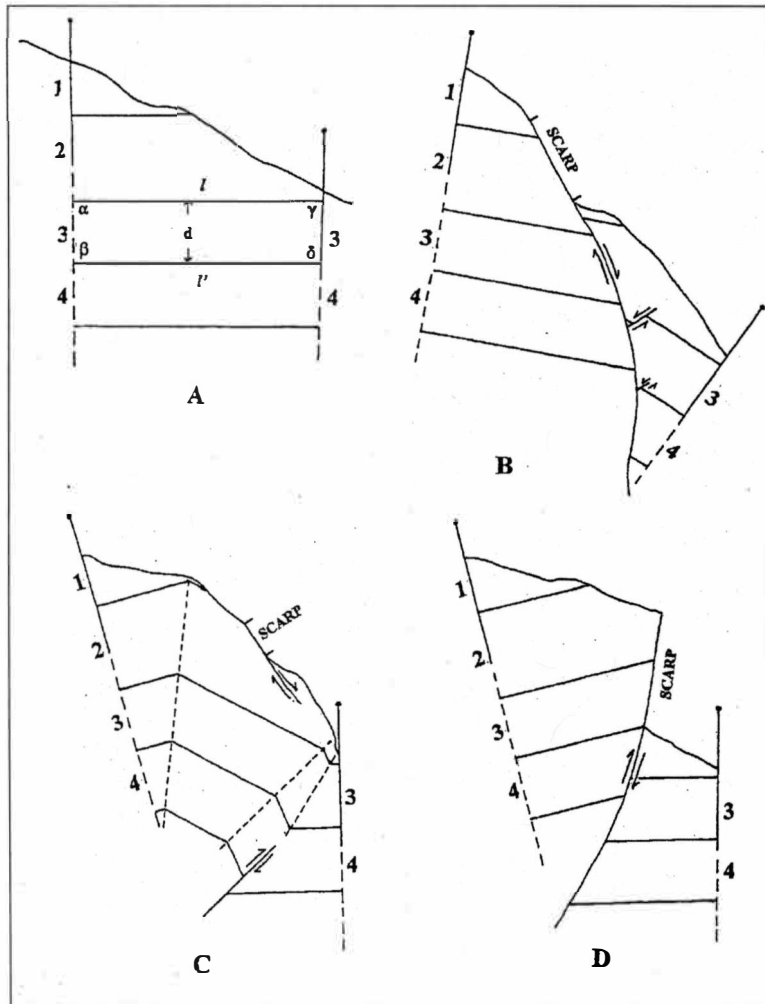


Figure 3. Cross section balancing illustration in which all original line lengths and angles are preserved. A) Originally there are two partial cells and two complete cells between poles. B) The poles diverge and differentially rotate resulting in a rotational normal fault plus two minor adjustment faults. C) The poles converge and differentially rotate resulting in a fault propagation fold structure. D) The same converging poles as in (C) result in an alternative rotational reverse fault interpretation. The choice between balancing methods (C) and (D) is dictated by the shape of the ground surface between poles and the best choice for the balancing of adjacent cells. (Chase et al., 2001a)

Source: Chase, R.B., Chase, K.E., Kehew, A.E., and Montgomery, W. W., 2001, Determining the kinematics of slope movements using low-cost monitoring and cross-section balancing: *Environmental & Engineering Geoscience*, 7(2), 193-203. Used with permission of Ronald B. Chase, author, 5-14-07.

surfaces or folds during the cross section balancing process. To maintain area balance,

the assumption is made that the soil volume remains constant, and that there is no mass movement oblique to the cross section. Although these assumptions are idealized given the inelastic nature of soils, they have little effect on model results (Chase et al., 2007a). The procedure described above for a slope segment is then applied repeatedly to an entire cross section. If the slump system is complex and develops many slip surfaces resulting in multiple fault blocks, the deepest block is balanced first. The section is then balanced progressively upward by balancing each block separately. If the blocks display the same magnitude and direction of displacement, it is reasonable to assume that only the deepest slip surface was active. For example, the cross section shown in Figure 2, was made along survey line 2 (Figure 4) after repeated surveys and cross-section balancing (Chase et al., 2007b). This slump system is complex and developed multiple fault blocks as shown in Figure 2B. Therefore, the deepest fault block was balanced first by using surface displacement data that were unique to it, and holding the other blocks fixed. Next the section was balanced progressively upward block-by-block, still maintaining the geometric rules discussed above. The end products were balanced cross sections where internal deformed geometries during progressive deformation were consistent with actual field observations (Figures 2B and 2C).

Although the cross-section balancing method produces accurate results, it is highly intuitive and extremely time consuming especially when dealing with multiple blocks (Chase et al., 2007a). There is, therefore, need for an efficient technique to digitally check the accuracy of the balancing and quantify any corrections required,

hence the use of Gaussian quadrature.

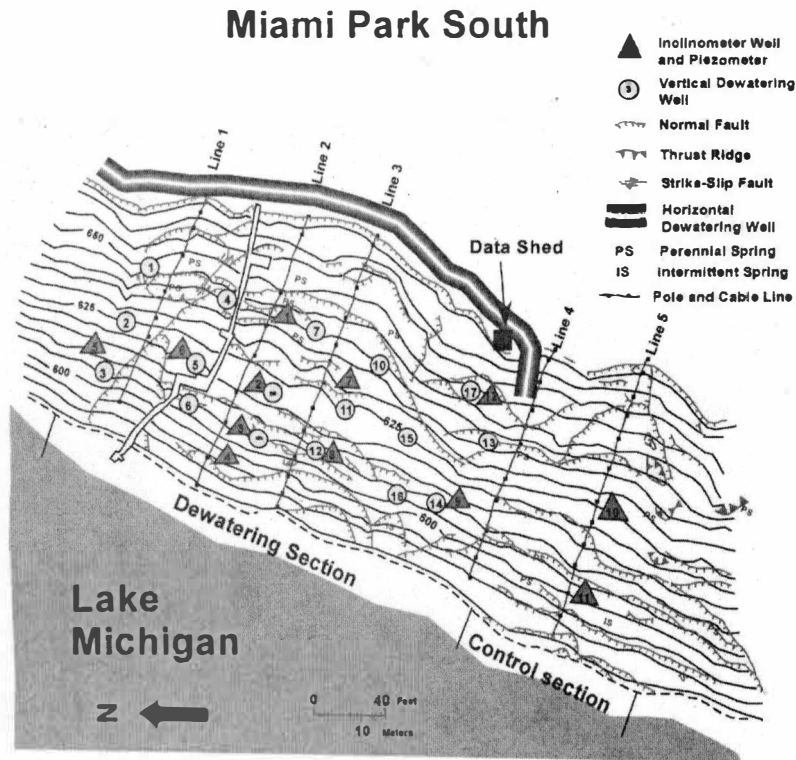


Figure 4. Map of study area showing positions of five pole-and-cable monitoring systems. The survey data for this study were obtained from Line 2.

The Use of Gaussian Quadrature

Gaussian quadrature is a form of numerical integration where the value of a univariate integral may be computed at different pre-selected integration points. For example, Table 1 shows two, three, and four such integration points for a special type of Gaussian quadrature called Gauss-Legendre rule (see Appendix). Numerical

integration is often necessary when an exact analytical solution (e.g. antiderivative) of the integral of a function does not exist or when dealing with discrete experimental data. In the latter case, where the function is unknown and is only defined by the experimental data, it is possible to implement a numerical interpolation. The nature of such an interpolation will depend on underlying assumptions made and available knowledge about the behavior of the function between the data. The oldest and simplest approach is polynomial interpolation (Kincaid and Cheney, 2002).

Table 1

Pre-selected points of integration and their associated weights for the Gauss-Legendre rule. Two, three and four different points are shown. Values can be readily obtained from mathematical tables.

N (Number of points)	Point, X_i	Weight, W_i
2	-0.57735	1.00000
	0.57735	1.00000
3	-0.77459	0.55555
	0.00000	0.88888
	0.77459	0.55555
4	-0.86113	0.34785
	-0.33998	0.65214
	0.33998	0.65214
	0.86113	0.34785

A detailed description of Gaussian quadrature is in the Appendix. Gaussian quadrature has been applied in several computational geoscience studies such as estimation of erosion rate variables (Arndt, et al., 2001), terrain corrections in GIS (Hwang et al., 2003) and describing groundwater flow in confined aquifers (Yeh et al., 2003), among others.

In this study Gaussian quadrature is used as a polynomial integration

technique to determine geometrical areas of stratigraphic segments in a structurally deformed profile. These areas are then compared with those in the original, non-displaced profile. The fundamental assumption is that for a two-dimensional slope, a stratigraphic boundary may be represented by an interpolating polynomial through fixed nodes in Cartesian coordinate space. This approach can be extremely useful especially if the resulting geometry of strata boundaries is too complex to confirm the line-length and angle measurements manually after the deformation has occurred. Such complexity is frequently observed in cases of displaced stratigraphy in lithologically heterogeneous terrain such as slopes composed of glacial deposits. Gaussian quadrature is a highly advantageous numerical integration technique because of the freedom in choosing pre-selected integration points leading to high accuracy. Additionally the Gaussian quadrature technique allows representation and manipulation of geometrical models in a digital format amenable to validation and analysis, as discussed below.

Using Gaussian Quadrature to Balance a Cross Section

To balance a cross section with Gaussian quadrature the initial and final profiles of the slope are required. A profile from the initial survey of the slope needs to be constructed showing original stratigraphic unit positions or cell boundaries. In this study these positions and boundaries were established with downward pole projections from the pole and cable system and horizontal reference lines as discussed above. After a period of structural deformation, the same slope is surveyed and its profile plotted from measured surface displacements. Stratigraphic layers are divided into segments whose areas are computed and compared for each profile. For example, the upper and lower boundaries of a stratigraphic-layer segment are shown

in Figure 5A. Since the shape of each boundary is known, the segment can be discretized into two interpolating polynomial functions (Figure 5B). The discretization can be conducted rapidly using a digitizing program to capture X and Y coordinates

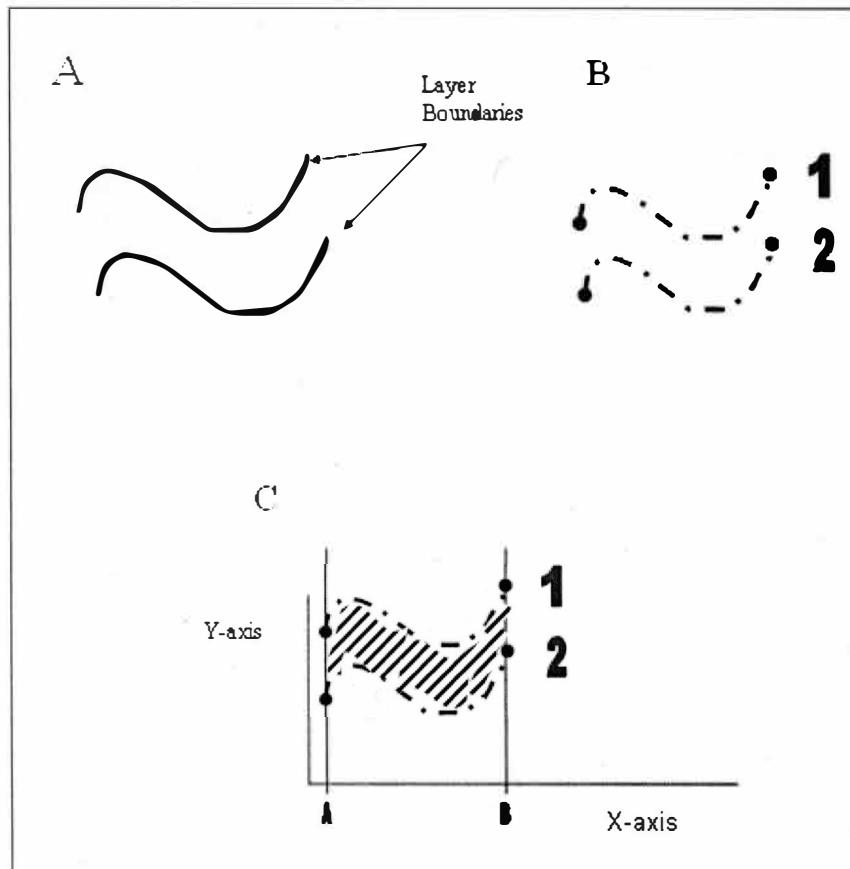


Figure 5. Layer boundaries. A) Discretization of a stratigraphic layer segment. B) The upper and lower boundaries of the segment are discretized into two interpolating polynomial functions. C) The difference between the integral of the upper polynomial and the lower polynomial is represented by the shaded region, which is equal to the area of the segment.

of selected points along each boundary. Since the integration of any function between

two points represents the area under its graph, the area of the layer segment in this case is the difference between the integral of Polynomial One and the integral of Polynomial Two represented by the shaded region between points A and B in Figure 5C. To integrate each function, the X and Y coordinates of the discretized points are put into the Gaussian quadrature equation (Appendix) with the aid of a spreadsheet program such as "Excel ®". The same spreadsheet program is used to subtract the integral of Polynomial Two from that of Polynomial One to calculate the actual area of the segment. The procedure illustrated in Figure 5 is repeated for the entire layer segments in a cross section. A sample of this spreadsheet is shown in Table 2 and is explained below.

Table 2

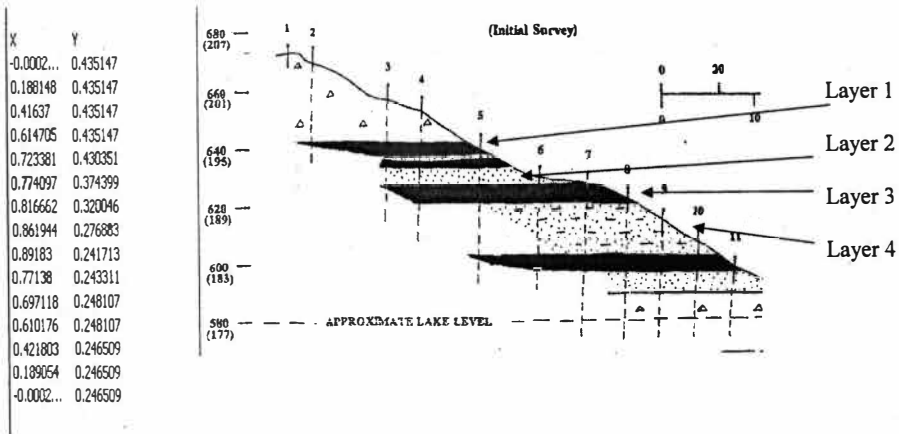
Gaussian Quadrature Spreadsheet for the first stratigraphic layer of lacustrine clay before and after deformation. Column A shows the Partition Number. For example the deformed layer was divided into three partitions. Columns B and C show the limits of integration, a and b , from Equation (5) (see Appendix A). Column D shows the pre-selected integration points, p . In Columns E, F and G are the new x coordinates and associated function evaluations obtained from digitization and Equation (6). Columns I and J are computation results using Equation (6) and weights from Column H. The balanced area is determined by simply subtracting Column J from I.

	A	B	C	D	E	F	G	H	I	J	K	L
1												
						Initial Layer 1						
2	Partition #	a	b	p	X	y1	y2	weight	Quad1	Quad2	Area	
3		0.00E+00	0.456218	-0.7745	0.051439	0.671744	0.572629	0.5555				
4	1	0.00E+00	0.456218	0	0.228109	0.671744	0.572629	0.8888	3.00E-01	2.61E-01	0.038657	
5		0.00E+00	0.456218	0.7745	0.404779	0.62	0.572629	0.5555				
6				-0.7745	0			0.5555				
7	2			0	0			0.8888	0	0	0	
8				0.7745	0			0.5555				
9				-0.7745	0			0.5555				
10	3			0	0			0.8888	0	0	0	
11				0.7745	0			0.5555				
12												
13									Total	Area	0.038657	
14						Deformed Layer 1						
15												
16	Partition #	a	b	p	X	y1	y2	weight	Quad1	Quad2	Area	
17		0.00E+00	0.299725	-0.7745	0.033794	0.677683	0.567072	0.5555				
18	1	0.00E+00	0.299725	0	0.149863	0.65	0.565469	0.8888	1.92E-01	1.69E-01	0.022736	
19		0.00E+00	0.299725	0.7745	0.265931	0.584706	0.557454	0.5555				
20		0.347339	0.472786	-0.7745	0.361483	0.48211	0.455	0.5555				
21	2	0.347339	0.472786	0	0.410063	0.486	0.397148	0.8888	0.059571	0.051931	0.00764	
22		0.347339	0.472786	0.7745	0.458642	0.45	0.4	0.5555				
23		0.447148	0.582667	-0.7745	0.462428	0.465	0.45	0.5555				
24	3	0.447148	0.582667	0	0.514908	0.472492	0.401957	0.8888	0.062897	0.057482	0.005415	
25		0.447148	0.582667	0.7745	0.567387	0.45	0.434	0.5555				
26												
27									Total	Area	0.035791	
28												

Gaussian quadrature was applied to the cross section along survey line 2 (Figure 4). The initial profile was constructed on June 10th, 1996 and assumed to consist of undeformed stratigraphic layers (Figure 2A). As displacement progressed, the profile shape was constructed repeatedly using the cell balancing rules described above. After seven years of ground movement, the deformed profile in Figure 2B was hand constructed from a June 10, 2003 survey. The four layers in Figure 6A were selected based on completeness and consistency. The layer segments bounded by strata and slip surfaces constructed from this survey were digitized carefully, to acquire

Cartesian coordinates, using the computer program ROCKWARE DIGIDATA (Figure 6) for both profiles. Results were then exported to an Excel® spreadsheet for area computations. The layer areas were determined using Gaussian quadrature rule by incorporating the mathematical formulation from Appendix A into the spreadsheet. An example of this spreadsheet format is shown in Table 2. The spreadsheet shows digital information for layer 1 in Figure 6A before and after deformation. This spreadsheet also incorporates equations from the Appendix used to conduct computations. These equations require parameters that are obtained from mathematical tables such as Abramowitz and Stegun, (1964). Column A shows the segment number while Columns B and C contain X coordinates from the digitizing program. The integration points from the mathematical tables are shown in Column D. Column E contains mathematical equations discussed in the Appendix that are used to perform the numerical integration. Columns F and G contain Y coordinates from the digitizing program. The weight parameters obtained from the mathematical tables have been put in H. Columns I and J also contain mathematical equations discussed in the Appendix. Segment areas are finally computed in Column K by subtracting results in Column J from those in Column I.

(A)



(B)

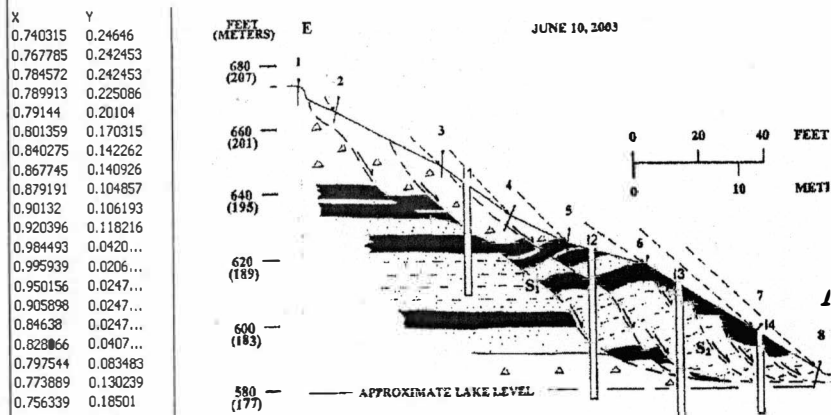


Figure 6. Digitization of the four stratigraphic layers. The coordinates are exported to an Excel[®] spreadsheet where Gaussian quadrature is applied to compute the area of each entire layer: (A) before and (B) after deformation.

Results of the Gaussian Quadrature Application to Line 2

The initial and final areas of the four stratigraphic layers before and after deformation as computed using Gaussian quadrature are shown in Table 3. For a stratigraphic layer to be considered as balanced, the value of the initial area must be as close as possible to that of the final area. The area differences between the initial and

final profiles for three of the layers are zero. The fourth layer shows a difference of 0.02 square units. Therefore all the layers balance, except for the fourth layer. This implies that the deformed segments of the fourth layer are missing 0.02 square units (approximately 13 percent) of the initial area. Because this deformed layer emerges at the toe of the slope (Figure 2C), we deduce that this missing section is due to erosion effects. However, if any of the other three layers had shown a significant difference between the initial and final areas, adjustments would have had to be made by the amount of square units missing in the spreadsheet program. This is because those layers would not have been subjected to toe erosion (see Figure 6). In this case, no adjustments are required to improve this cross section because it is properly balanced.

Table 3

A comparison of initial and final layer areas obtained from Gaussian quadrature spreadsheets in units squared. Areas for Layers 1, 2 and 3 (numbered in Figure 6A) before and after deformation are well balanced. The special case for Layer Number 4 is discussed in the text.

Layer No.	Initial Unit Area	Final Unit Area	Difference
One	0.04	0.04	0
Two	0.03	0.03	0
Three	0.05	0.05	0
Four	0.15	0.13	0.02

Application to the Process of Slope Stability Analysis

The initial and deformed stratigraphic layer positions and cell shapes are dramatically diverse (Figure 6A and 6B). Therefore, a limit equilibrium analysis based only on initial conditions, without taking into account the deformations, would

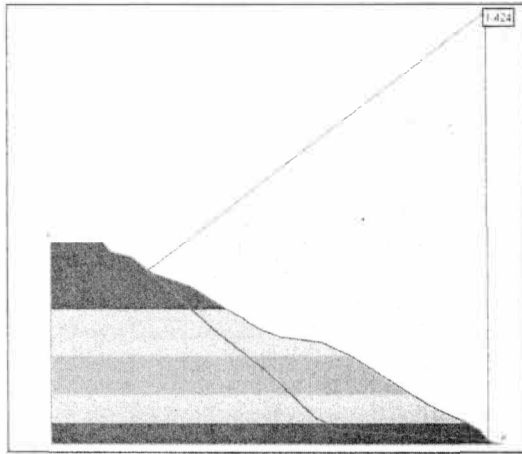
yield different results from an analysis that includes the geometry of deformation. Limit equilibrium analyses of this slope were conducted using field geometric conditions as represented initially on June 10, 1996 and geometric conditions precisely seven years later. Geotechnical parameters (Table 4) were obtained from consolidated-undrained tests on samples of onsite soils (Montgomery, 1998). Janbu's simplified method (Janbu, 1968) was implemented using the computer program, SLIDE. This method was chosen because it is applicable to any shape of slip surface. The results for an effective stress analysis are shown in Figure 7. Profile (A) yields a safety factor of 1.4 while Profile (B) yields a safety factor of 1.2. These values agree with actual field observations. Clearly a change in subsurface geometry and mass of the slide block reduced the safety factor. From these results we can infer, with the aid of geometric and mathematical modeling, that the landslide became less stable during the seven year time frame.

Table 4

Effective stress geotechnical parameters used for the slope stability analysis. Values shown for the defined stratigraphic layers: diamicton (glacial till), sand, Lclay (lacustrine clay), ILSAC (sand/clay) were obtained from Montgomery (1998).

Soil Layer	Unit weight (kN/m ³)	Cohesion (kN/m ²)	Phi (degrees)	Void ratio
Diamicton	19.3	0	28	0.35
Lacustrine clay	15.7	0	20	0.67
Sand	20.4	0	34	0.32
Inter-layered sand & lacustrine clay	20.4	0	34	0.49

(A)



(B)

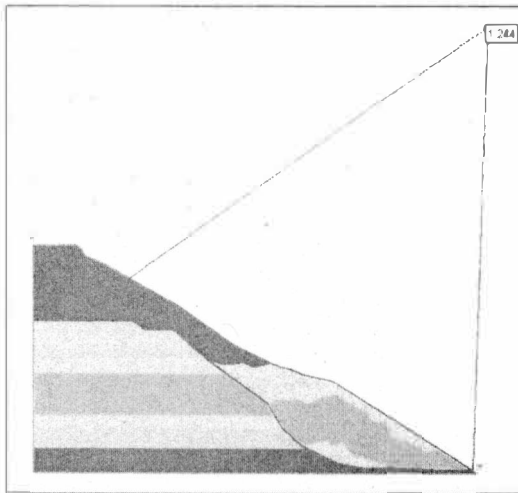


Figure 7. Limit equilibrium analysis results of slope using geometric field conditions: A) June 10, 1996; B) June 10, 2003. The analysis was conducted using the most critical slip surface from Figure 6B

Conclusions

Gaussian quadrature has been successfully used as a quality control tool for section-balancing the subsurface geometries of a slope undergoing progressive failure.

Geometric combinations of cell segments defined by stratigraphic units and estimated slip surfaces were cross-section balanced by conserving geometrical areas before and after deformation. The original profile and the final deformed profile were also subjected to a slope stability analysis using Janbu's method and effective stress to demonstrate the important role played by accurately defined geometry. The results show a significant difference in safety factors with the deformed profile proving to be less stable. The Gaussian quadrature technique allows representation and manipulation of geometrical models that allows digital validation. This provides a crucial bridge between a geometric investigation and the establishment of mitigation/engineering strategies for stabilization of a section-balanced slope.

CHAPTER III

SOME APPLICATIONS OF NEURAL NETWORK MODELING IN ACTIVE SLOPE PROBLEMS

Introduction

Slope stability is important because slope failures or landslides can lead to the loss of life and property. Current direct and indirect costs of slope failures exceed \$1 billion annually in the United States alone. Limited data and unclearly defined problems often complicate the study of landslides (Nieuwenhuis, 1991). A special type of active landslides known as earthflows/slumps have always posed a unique challenge to the geotechnical, engineering geology and geomorphology community because they are almost impossible to study using conventional slope stability analysis techniques such as limit equilibrium. For example, factors of safety exceeding one do not guarantee stability for these types of mass movements, and neither do values less than one always imply failure. In earthflows, slope movement is in the form of progressive ground failure (Chowdhury, 1978, Suemine, 1983, Kamai, 1997, Petley et al., 2005). Furthermore, displacement may occur along more than one “critical” slip surface. To compound the problem, failure along such a complex network of slip surfaces may occur gradually or catastrophically.

Previous studies have introduced useful strategies capable of addressing these challenges including, but not limited to, finite elements (Griffiths and Lane, 1999), statistical or probabilistic techniques (Griffiths and Fenton, 2004), multiple and global (universal) safety factors (Baker and Leshchinsky, 2001), alternative, non-laboratory based geotechnical modeling parameters (Kamai, 1998, Stark et al., 2005), and others.

Finite element analysis can often be complex and time consuming, even though the results may be accurate and more meaningful than limit equilibrium analysis in some cases (Duncan, 1996a). Statistical methods often require physical or mathematical models showing clear functional dependence of outputs on model parameters (Neaupane and Achet, 2004). The common feature of the above methods is that they are physics-based, implying mathematical formulation of fundamental laws. The underlying disadvantages with this approach include a) failure to assess slope stability in the absence of geometry and soil properties pertaining to the formulation, and b) difficulty in representing actual ground truth conditions (Cao, 2002). Artificial Neural Networks on the other hand are solely based on laboratory and/or field data because—in perhaps one of the most powerful features of neural networks—of their ability to map complicated functional relationships between dependent and independent variables without any *a priori* assumptions regarding dependency, unlike most curve fitting techniques (Liu et al., 2006).

The behavior of creeping landslides is clearly highly non-linear and time-variant due to a complex combination of internal and external variables. Internal variables include those related to the material itself such as shear and cohesive strength, or strain and soil particle structure. External variables include factors such as precipitation, groundwater, and temperature conditions. The objective of this study is to apply a heuristic approach that inherently addresses such variables by using Artificial Neural Network modeling. The relatively new field of Artificial Neural Networks has been previously used in geotechnical engineering, such as site characterization of soil properties (Juang et al., 2001), prediction of unsaturated soil behavior based on triaxial tests (Habibagahi and Bamdad, 2003), and prediction of factors of safety from geotechnical parameters (Wang et al., 2005), among others.

Unlike most models, neural networks have the ability to learn and improve their performance.

For this study three categories of Artificial Neural Network models are investigated: using displacement data to predict slip positions, using climate data to predict groundwater levels and using climate and ground water data to predict displacements. All neural network models are developed and assessed in the context of real field data.

Artificial Neural Networks (ANN)

An ANN is a mesh of computing nodes and connections, fashioned after the biological nervous system. The nodes are the basic processing elements which can be trained to map data non-linearly once they are activated (“turned on”). A popular choice for a widely applicable activation function is the sigmoid function, or logistic function: $y = 1 / (1 + e^{-x})$. These nodes or artificial neurons are often organized in layers: input, hidden and output layers as portrayed in Figure 8. Each connection is assigned a numerical value, known as a weight, which can be changed during neural network training. An advantage of ANN over physics-based models is their ability to learn complex relationships among data sets. Once this knowledge is acquired, they may be applied in instances where new data do not completely define the system. An ANN does not rely upon the physical laws of the system it is modeling. This is an advantage over physical-based models because information about the physical parameters of the system is not required. The accuracy of an ANN can be assessed by the mean squared difference between actual and predicted or output values (Root mean squared error or RMSE):

$$RMSE = \sqrt{\frac{\sum_{i=1}^T (error)^2}{T}} \quad (1)$$

where T is the sum of the individual i nodes.

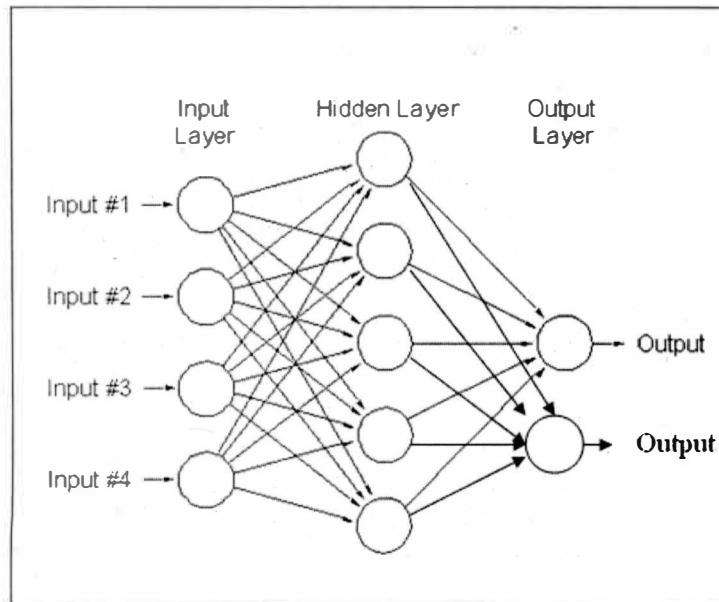


Figure 8. Artificial Neural Network layered arrangement of input, hidden and output nodes in a Multi Layer Perceptron (MLP) or feed forward architecture.

The objective in ANN modeling is to minimize this error with respect to the connection weights. This process is known as “learning” and several learning algorithms exist in the literature (Poulton, 2001). The learning algorithm used in this study is a combination of back propagation and adaptive gradient. Back propagation is a gradient descent method that searches for the global optimum of the network weights (Rumelhart et al., 1986). First, partial derivatives of the errors with respect to each weight in the network are computed as described in Appendix B. Then the weights are modified as follows:

$$\Delta \omega_{ij}(t) = \eta \delta_j o_i + \alpha \Delta \omega_{ij}(t-1) \quad (2)$$

where:

$\omega_{ij}(t)$ = weight of the unit ij at time t

η = the learning rate

δ_j = the local error gradient

α = the moment coefficient

o_i = the output of the i^{th} unit

Details of how these parameters pertain to the back propagation algorithm are described in the Appendix.

Predicting Slip Surface Locations from Displacements with Artificial Neural Networks

The Problem of Slip Surface Location

Investigations of active slopes frequently include determination of slip surface locations. This can be achieved by using either field methods or modeling techniques. Field methods include drilling, trenching, mapping, inclinometer profiling, and geophysical techniques such as ground penetrating radar and seismic surveys. Because field studies can often be expensive and time consuming, modeling techniques provide a viable alternative. Modeling techniques include geometric modeling (viz. subsurface extrapolation from surface markers), finite elements, limit equilibrium and optimization algorithms. Unfortunately, these modeling techniques

may also produce highly subjective results influenced by prior user assumptions. Because ANNs learn relationships of a system independently, they can be applied to the problem of slip surface detection with minimum human interference.

Data Acquisition

To develop a reliable ANN model that predicts slip surface positions, true field data must be used. The data must include displacements and some known slip surface depths. In this application, field data were acquired from drill logs and slope surface displacements at a site called Miami Park South (MPS) along the southeastern shoreline of Lake Michigan (Figure 9).

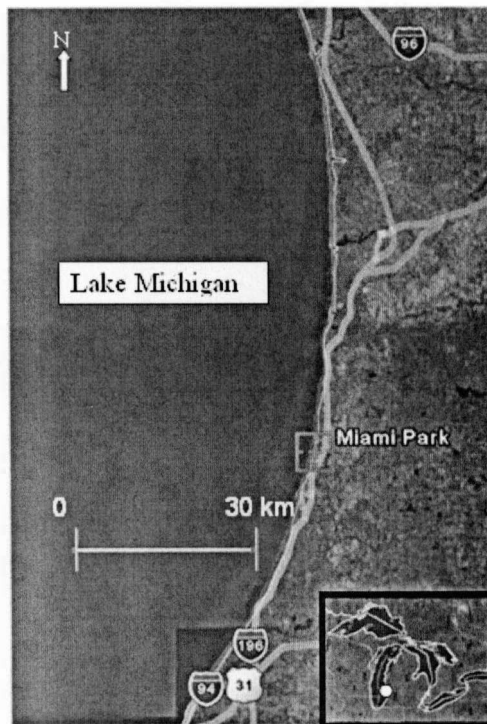


Figure 9. Location of the Miami Park South site

The drilling was conducted in the summer and fall of 2003 to install 17 dewatering

wells, 12, inclinometer wells and 14 vibrating wire piezometers as part of a dewatering experiment conducted jointly by Western Michigan University and the US Army Corps of Engineers. The vertical depths of the wells ranged from 25 feet (7.6 m) to 52 feet (15.85 m). Split spoon sampling was conducted every 5 feet (1.52 m), with decreased sampling intervals where necessary. Surface displacements were recorded by five survey lines consisting of eight-foot (2.5 m) fence poles vertically driven about five feet (1.5 m) into the ground and placed down the slope face in near-parallel rows (Figure 10).



Figure 10. The pole-and-cable slope displacement monitoring system (described in Chase et al., 2001a). Measurements from the system are used to compute neural

network training parameters.

A steel cable marked with colored plastic tape at 1.5 inch (3.8 cm) intervals runs through each pole from the crest of the slope to the toe. Tri-weekly surveys of each row involve the measurement of distances between poles, cable height above ground at each pole, cable angles between poles, and pole inclination angles along the strike and down the dip of the slope. This information is used to calculate ground translations, rotation and ground elevations relative to a fixed benchmark at the top of the slope. These field measurements have been compiled into a ten-year data base that has been used for analysis of the movement history and geometric evolution of the slopes (Chase et al., 2001b, 2007a), (Figure 11A). This data base was used to construct the training file discussed in the next section.

Artificial Neural Network Training and Testing

The database described above was used to compose the training file illustrated in Table 5. The table consists of columns showing seven different variables --six inputs and one output parameter for a number of locations. Input variables include cumulative ground displacement, cumulative ground elevation change, cumulative ground rotation along the dip and strike of the slope, and soil type. Each of these parameters is defined and calculated as follows:

- a) Cumulative ground displacement = total distance moved by the ground (and pole) at the base of each pole.
- b) Cumulative ground elevation change = change from initial ground elevation.

c) Near-surface ground rotation (parallel to dip) = deviation from initial pole inclination angle. Positive values indicate forward rotation, while negative values indicate back rotation.

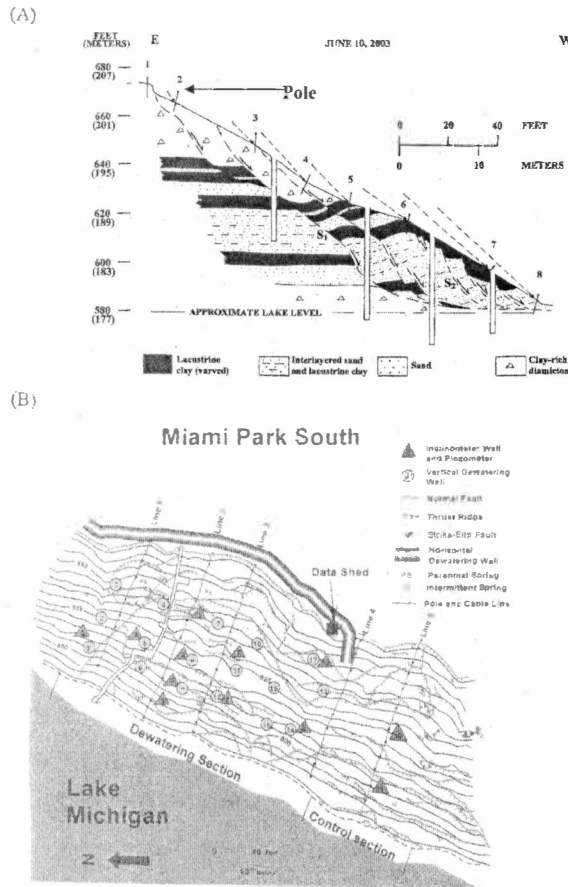


Figure 11. Slope geometric evolution. A) Slope profile cross section along the pole-and-cable line 2 (shown in Figure B), constructed from geometric modeling of surface displacements and validated by drill logs conducted in June 2003. The vertical distances to the nearest slip surface are used to train and test the neural network. B) Map of the Miami Park South site (Figure 9) showing the location of pole-and-cable line 2.

d) Near-surface ground rotation (parallel to strike) = deviation from initial pole inclination angle.

e) Pole soil type = soil type pole installed in (sand, clay or till).

f) Slip surface soil type = soil type of anticipated slip surface location, if known (sand, clay or till).

Table 5

Sample training file from MPS. A= Cumulative ground displacement, B=Cumulative ground elevation change, C=Ground rotation (parallel to dip) D= Ground rotation (parallel to strike), E=Pole location soil type, F=slip surface location soil type (1=Till, 2=Clay, 3=Sand), and G= Closest slip surface vertical depth.

A (ft)	(m)	B (ft)	(m)	C (deg)	D (deg)	E	F	G (ft)	(m)
-1.35	-0.41	0.00	0.00	3	1	1	1	10	3.05
-2.25	-0.68	-0.27	-0.08	0	2	1	1	15	4.57
-0.77	-0.24	2.75	0.84	16	3	1	1	0	0.00
7.58	2.31	-0.55	-0.17	65	30	1	1	8	2.44
-1.34	-0.41	-0.91	-0.28	49	30	1	1	8	2.44
1.96	0.60	-0.92	-0.28	-1	-1	1	3	40	12.19
5.33	1.62	-0.09	-0.03	5	-2	1	3	40	12.19
1.67	0.51	-1.29	-0.39	1	-3	2	3	36	10.97
1.22	0.37	-0.74	-0.23	0	-2	2	3	20	6.10
-3.94	-1.20	-1.10	-0.34	2	-2	2	3	14	4.27
-10.80	-3.29	-1.47	-0.45	5	1	2	3	12	3.66
-11.96	-3.64	-1.47	-0.45	12	10	2	3	16	4.88
5.40	1.65	0.37	0.11	11	10	1	1	10	3.05
15.10	4.60	1.37	0.42	3	6	1	1	4	1.22
24.88	7.58	-1.84	-0.56	25	1	1	1	4	1.22
17.19	5.24	-0.27	-0.08	8	1	1	2	8	2.44
8.52	2.60	-0.18	-0.05	5	7	2	2	14	4.27
37.50	11.43	-0.73	-0.22	3	5	2	2	2	0.61
0.58	0.18	0.00	0.00	6	0	1	1	4	1.22
-0.58	-0.18	0.19	0.06	2	-1	1	1	4	1.22
0.83	0.25	0.19	0.06	5	2	1	1	4	1.22
3.67	1.12	0.00	0.00	58	30	1	1	20	6.10
0.81	0.25	0.00	0.00	0	2	1	1	14	4.27
1.69	0.51	-0.10	-0.03	0	1	1	2	10	3.05
1.56	0.48	0.00	0.00	1	2	1	2	12	3.66
2.23	0.68	0.18	0.05	5	4	1	3	22	6.71
9.06	2.76	-0.18	-0.05	72	30	1	2	16	4.88

The output parameter (G) is the vertical depth from the ground to the slip surface. In the case of multiple slip surfaces such as Figure 11, then the output is the vertical depth from the ground to the first slip surface encountered. Consequently, if the sampling of ground displacements/rotations is limited in the case of multiple slip surfaces, the ANN prediction could result in ambiguity. This problem can be addressed by sampling the ground displacements/rotations at closer spaced intervals. A limit of the ANN method is therefore the availability of field data: the greater the amount of data the higher the chances of successful slip surface characterization.

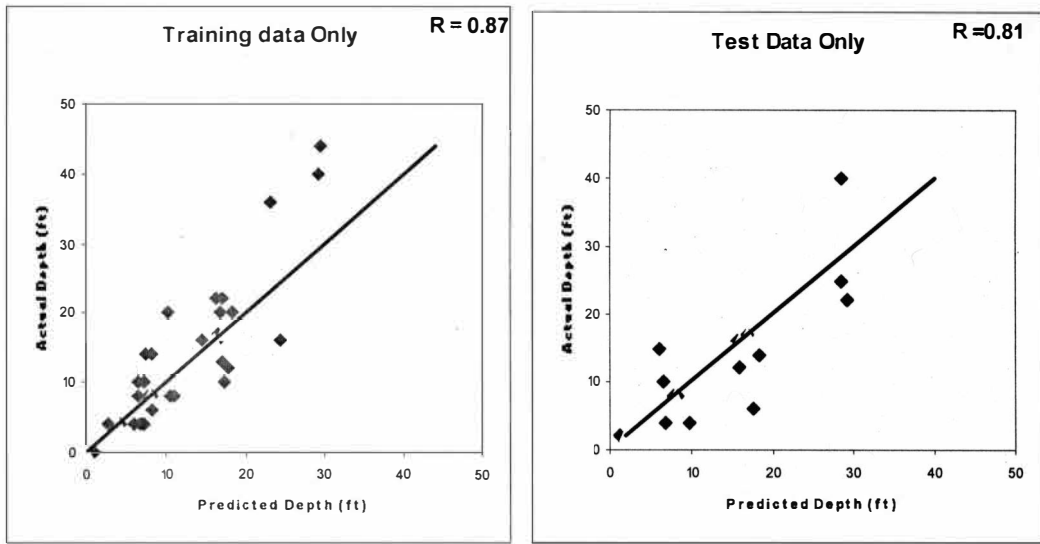
The ANN uses the training file in Table 5 to learn to associate the input variables with the expected output variable in Column G row by row. After each successive iteration, the model checks its performance by comparing its output with the expected one, and computing an error. The model then adjusts its internal connection weights using the learning rule in the Appendix until this error is minimized. Duration of this training phase depends on the size of the training file and computer processor speed. Once training is accomplished, the neural net is ready for testing or validation (Figure 12). New input parameters are provided to the model to predict outputs. The results are checked against actual known values to assess whether the model is acceptable or needs refining. If model predictions are acceptable then the neural network is ready for use.

To train the neural network, the back propagation algorithm discussed above was implemented using the commercial software NEURALWORKS PREDICT. A sigmoid output function was also used. The training file consisted of thirty three patterns (or data sets) derived from the slope displacement database discussed above. For validation, the model was first tested on fifteen new data sets it had not yet

“seen”. The model was again tested using a total of forty-eight patterns consisting of

A)

B)



C)

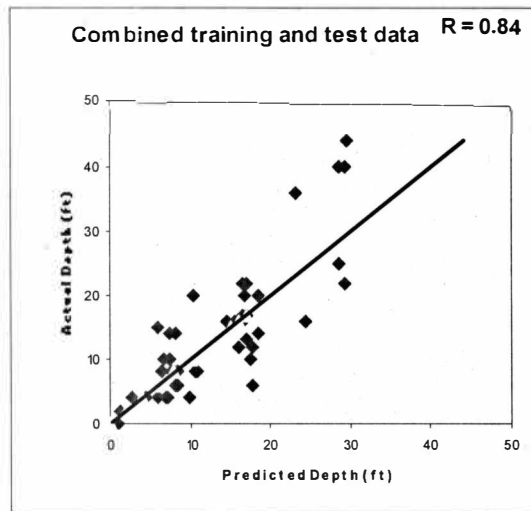


Figure 12. Neural network training and test results. The model predictions are compared with actual data for three cases. A) Only data used during neural network training; B) only data used to test the neural network model; and C) using both data from (A) and (B).

both old and new data. Results are shown in Figure 12 and discussed in the next section. In summary the steps for supervised neural net learning and testing are:

1. Select and prepare input and output parameters from raw data and create a training file (Table 5).
2. Create neural network model architecture (Figure 8).
3. Input training file into the model.
4. Initiate training by implementing the back propagation algorithm (see Appendix).
5. Continue neural network training until errors are minimized.
6. Test model on new data for validation.
7. Refine model if necessary.
8. Model ready for use.

Results of the Artificial Neural Network Testing for Miami Park South

The Miami Park South site has an average long term rate of recession of 1.3 ft (0.39 m) per year. The bluffs at the site have an average height of about 80 ft (24 m), and a slope angle of about 34 degrees. The geology consists of glacial diamicton (till), and layers of sand and clay, as shown in Figure 11. The displacement geometries are also shown.

When tested, the ANN predicts slip surface depths closely matching observed ones (Figure 12). A common linear trend is observed for all three cases described. Pearson's correlation coefficient, R , is the linear correlation between target and predicted values. Perfect correlation gives an R value of 1.0. Anticorrelated outputs

have an R value of -1.0. Uncorrelated output gives an R value of 0.0. The acceptability of an R value may vary depending on problem domain. For example, for some noisy domains, R values of less than 0.5 may be considered good. The training data in Table 2 show a stronger correlation ($R=0.87$) than the test data ($R=0.81$) because of the supervised nature of the learning. This implies the model predicts familiar data better than it does new data. The predicted overall test results fitted to field data are shown in Figure 13. There is a close match between model output and actual depths, especially for depth values less than 30 ft (9 m).

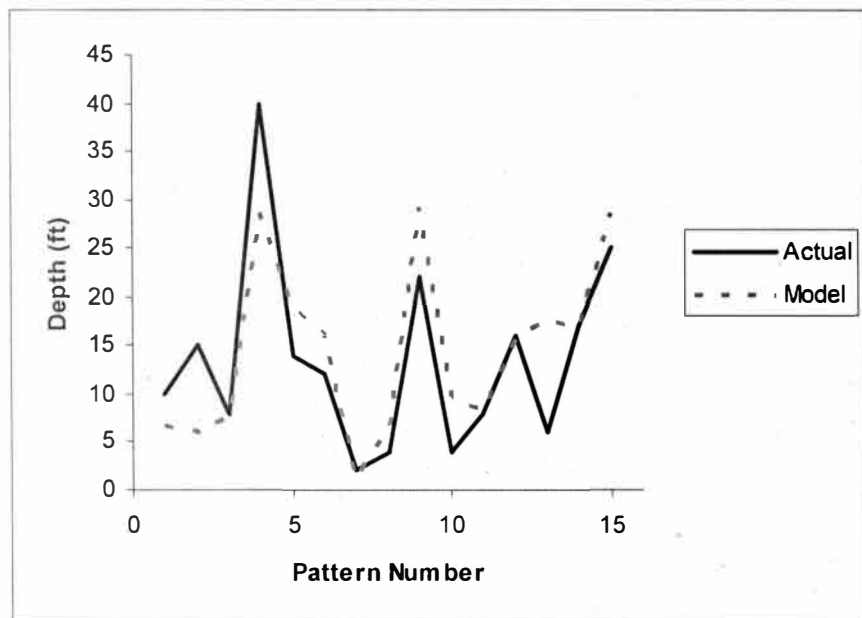


Figure 13. Model fit showing predicted slip surface depths versus true depths for test data. The x-axis shows the pattern number (or data point); the y-axis shows the depth. Pearson's correlation coefficient R for all test data is 0.81.

Error analysis provides a quantitative assessment of the ANN predictions. In Table 6 "Avg. Abs." represents the average absolute error between target output and predicted value. RMS is the root mean square error between the target output and the

predicted output. Confidence Interval represents an error bar around the output. For example if a 95% confidence level is used, then we can have 95% confidence that the predicted output will be within X of the target output value, where X is the confidence interval. The assumption made is that the test set is representative of the data population. In this case there is an average absolute error of about 1.3 m and a root mean square error of 1.8 m, as shown in Table 6. Also there is 95% confidence that the predicted slip surface depths-magnitudes are within 3 m of the actual values. This error analysis explains the observed fits in Figures 12 and 13.

Table 6

Summary statistics for neural network training and testing for slip surface depth prediction. R = Pearson's correlation coefficient, Avg Abs = the average absolute error, Max Abs = maximum absolute error, RMS = the root mean square error, Conf. Interval = the confidence interval and Records is the number of data sets used.

Statistic	R	Avg. Abs. ft (m)	Max. Abs. ft (m)	RMS ft (m)	Conf. Interval (95%) ft (m)	Records
Train	0.87	4.09 (1.25)	14.5 (4.42)	5.46(1.66)	11.1 (3.38)	33
Test	0.81	4.35 (1.33)	11.73(3.57)	5.8 (1.77)	11.1 (3.38)	15
All	0.84	4.17 (1.27)	14.5 (4.42)	5.57(1.69)	10.7 (3.26)	48

Sensitivity Analysis for the Slip Surface Prediction

A sensitivity analysis was conducted to investigate the significance of each of the model input parameters. The ranking system was based on ratios which were computed as follows (Coppola, 2005):

$$\text{Ratio} = \frac{\text{RMS error of ANN without input parameter during prediction}}{\text{RMS error of ANN with input parameter during prediction}}$$

The input parameter with the highest ratio was given a rank of “one” implying highest significance. Conversely, the input parameter with the lowest ratio was given a rank of “six.” Sensitivity analysis results, summarized in Table 7, show that the soil type which the slip surface penetrated was the most significant input parameter for the prediction.

Table 7

Sensitivity analysis for slip surface depth prediction. CD = cumulative ground displacement, CGE = cumulative ground elevation change, GR1 = Ground rotation (parallel to dip of slope), GR2 = Ground rotation (parallel to strike of slope), PST = pole position soil type, SST = slip surface position soil type, RMSE = model root mean square error when particular input parameter is omitted, Ratio = RMSE when particular input parameter is omitted to RMSE when all six input parameter are included

Statistic	CD	CGE	GR1	GR2	PST	SST
Rank	6	5	3	4	2	1
RMSE	6.07	6.18	6.28	6.25	7.55	9.53
Ratio	1.11	1.13	1.15	1.14	1.38	1.74

Cumulative ground displacement was the least significant input parameter by rank. It can also be deduced from Table 7 that cumulative ground elevation change was a more important predictive parameter than cumulative ground translation, and that ground rotations were important as well, especially for down dip movements. The former observation is probably due to significant vertical activity relative to horizontal translation during most of the sliding, while the latter observation is probably due to rotational failure in a down-dip direction. Rotational failure is typical in clayey or cohesive slope materials (Chen, 1975). Generally speaking, all of the six input parameters have a unique contribution to predicting the precise location (i.e.

depth) of a shear plane as noted from the RMSE values during sensitivity analysis. Therefore if any of the inputs are missing, predictions can still be made by adjusting the model accordingly. This is demonstrated in the next two examples.

Example 1: La Mure Landslide, French Alps

Description

The model developed above was applied to a landslide problem in the French Alps (Figure 14) near Grenoble investigated by Van Genuchten and Nieuwenhuis (1990). The landslide, developed in varved clays, exhibits behavior not explainable using classical 2-D stability analysis. Its movements are known to be greater than one meter per year. The dimensions of the study area are about 500 m long and 125 m high. Soils consist of mostly over-consolidated silty clays with residual (weakened) shear strengths. The landslide is active, the geometry and soils are known, and displacements occur along existing slip planes and movements are detectable. Field instrumentation included a geodetical network of surface markers and flexible tubes for displacement measurements, piezometers for groundwater level detection, and meteorological equipment. This landslide has seasonal movements driven by excessive precipitation or snow melt. Its hydrology is complex due to the presence of scarps and fissures.

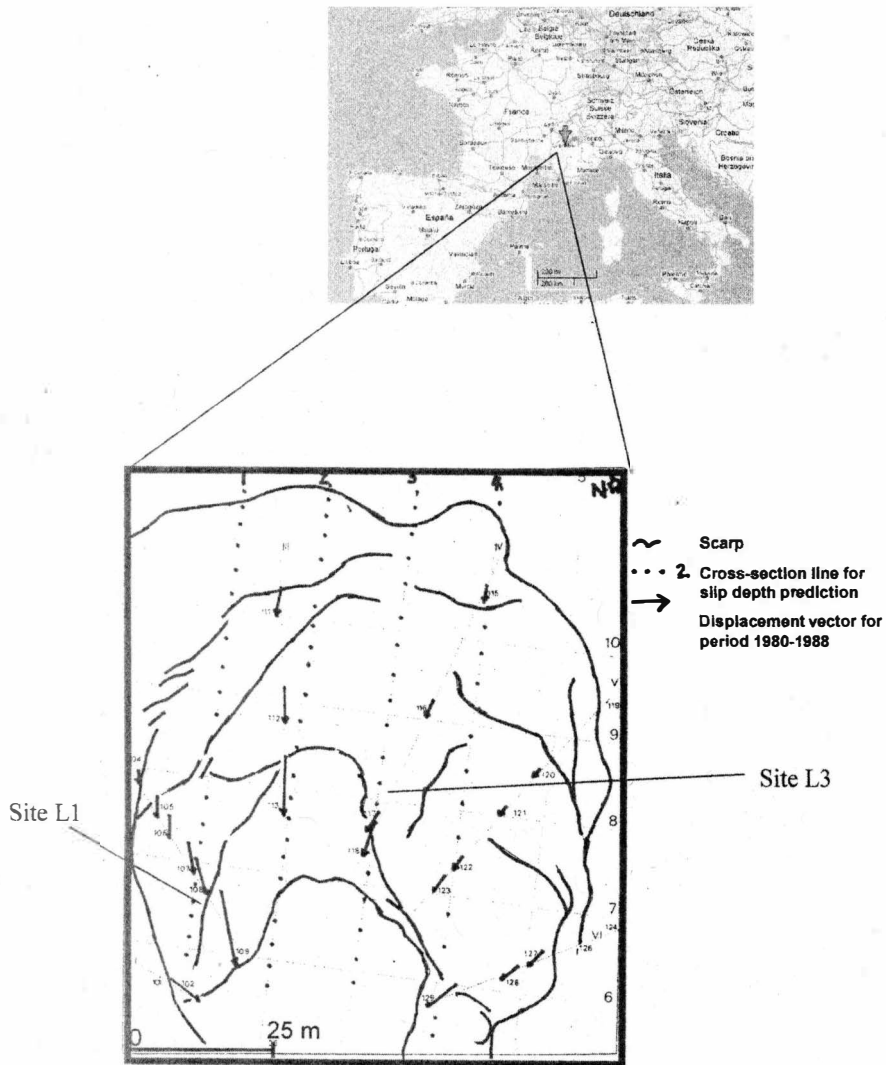
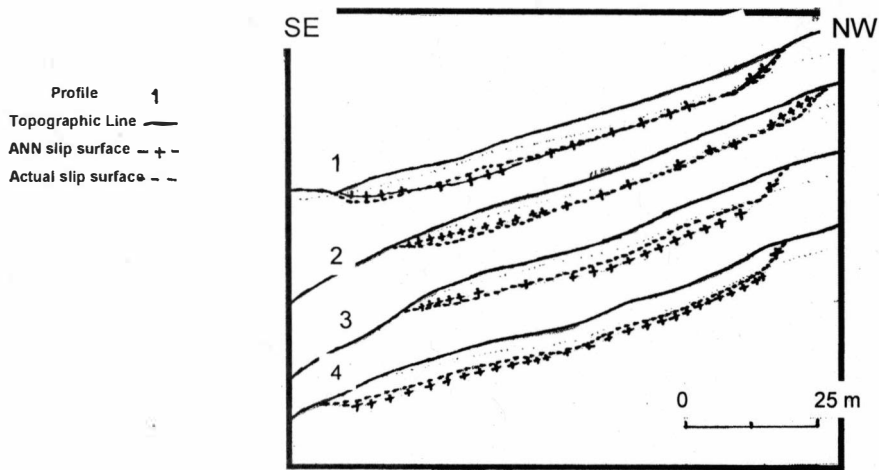


Figure 14. The La Mure Landslide in the French Alps. The ANN prediction of slip surface positions was conducted along the four slope cross section lines shown. Sites L1 and L3 are discussed in text Example 3. (modified from Van Genuchten and Nieuwenhuis, 1990)

Artificial Neural Network Model Set Up for the La Mure Landslide

The neural network model discussed above was developed using six input parameters (Table 5). However the La Mure landslide case study only has four of these available: ground rotations in the strike and dip directions of the slope were missing. The goal was to test the ANN prediction using only four input variables. Cumulative ground displacements and cumulative ground elevation changes were obtained from horizontal and vertical displacement vectors. These values were normalized to fall between zero and one so that the model trained on data from a different site (MPS) could be applicable. Soil parameters were put into the model iteratively to determine which values corresponded to those from MPS. The back propagation algorithm discussed above was implemented using the commercial software NEURALWORKS PREDICT. A sigmoid output function was also used. The results of the predicted slip surface positions for four profiles show a close match with measured positions (Figure 15A). There is still significant scatter (Figure 15B), however, probably due to the missing ground rotational input parameters. A limit equilibrium critical slip surface search using Bishop's method for the four slopes is shown for comparison in Figure 16. The safety factor values for the search lie between 0 and 1.5. It can be seen that the ANN model provides less slip surface prediction ambiguity than does the limit equilibrium search.

A)



B)

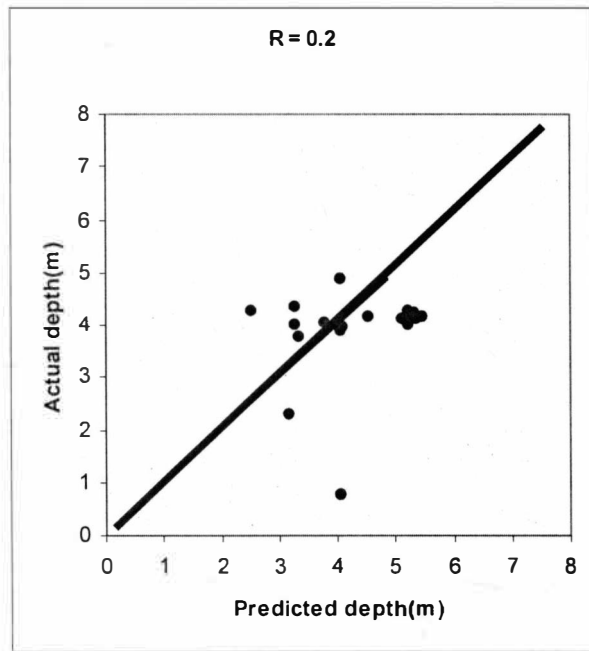


Figure 15. Slip surface predictions for La Mure. A) Predicted versus true slip surface positions for the four slope profiles located in Figure 14. (modified from Van Genuchten and Nieuwenhuis, 1990). B) The scatter of the predicted values around the true fit is also shown.

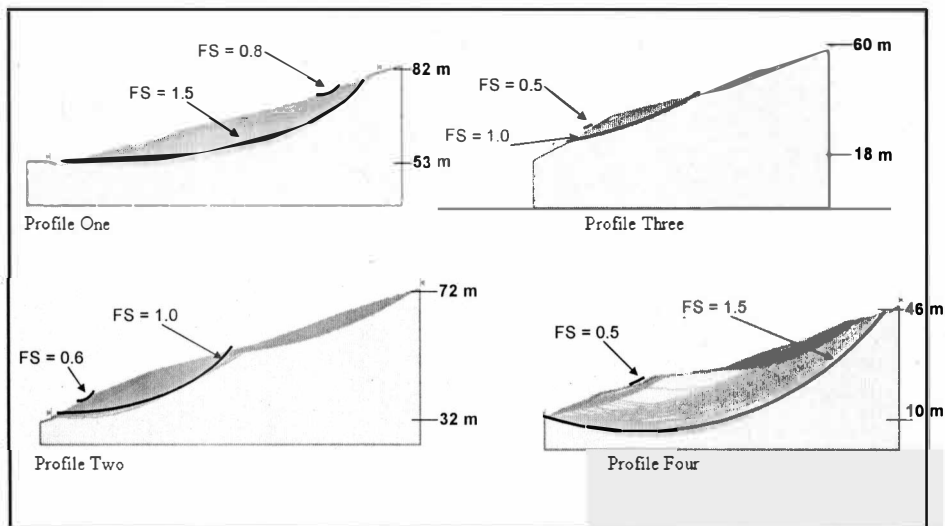


Figure 16. Critical search for slip surface using limit equilibrium analysis and Bishop's method for the four slope profiles shown in Figure 14. The dark lines show the lowest and highest factors of safety for the critical search.

Example 2: Mam Tor Landslide, Derbyshire, England

Description

The Mam Tor landslide was studied by Skempton et al. (1989) and more recently by Rutter et al. (2003). The landslide exhibits episodic and creep movements leading to a collapse of the eastern section that has left an 80 m high scar. The dimensions of the slipped mass are about 750 m long and 500 m wide (Figure 17). The geology consists of mostly mudstone overlying sandstone. The average displacement rate is 10 cm per year, with the central region moving faster at 50 cm per year. Displacements have also been known to correlate with annual variations in rainfall above a critical threshold level. Displacement monitoring was conducted between 1996 and 2002 using a total of 38 stations (Rutter et al., 2003). The stations were measured using a Geodimeter 408 electromagnetic distance measurement

(EDM) instrument. The instrument measured horizontal and vertical movements relative to a bench mark.

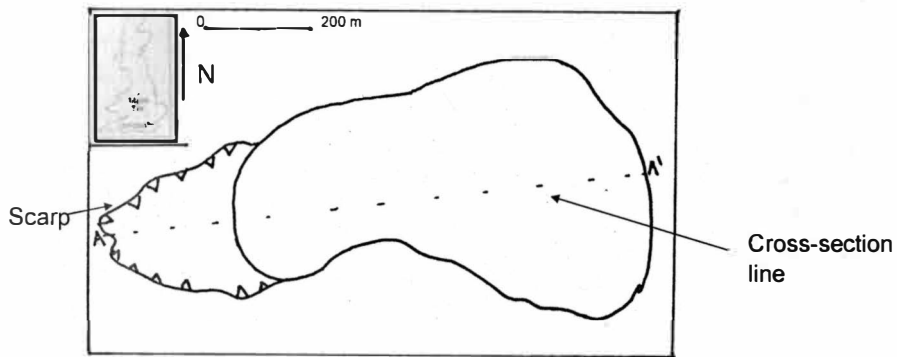
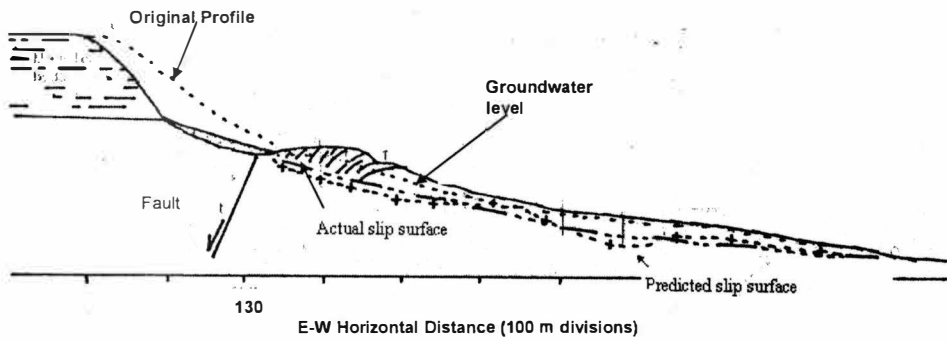


Figure 17. Location and aerial map of the Mam Tor Landslide in Derbyshire, England. The ANN prediction of slip surface depths was conducted along AA'

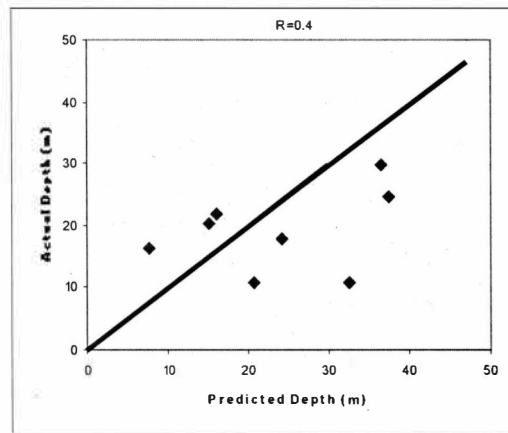
Artificial Neural Network Model Set Up for the Mam Tor Landslide

The neural network model discussed earlier was adapted to the Mam Tor landslide by using the locally available data for neural net training and validation. The input parameters used were cumulative ground displacement and cumulative ground elevation change, while the output parameter was vertical depth to the slip surface. Ground rotations in the strike and dip direction of the slope, and soil types were left out because they were unavailable. The back propagation algorithm was again implemented using a sigmoid output function. After training, the ANN model was validated using an independent data set from Mam Tor. The results of the predicted compared to measured slip surface position are shown in Figure 18A. Although there is significant scatter (Figure 18B), the fit is still better than a limit equilibrium search (Figure 18C). The scatter is probably because the ANN model utilizes only two input parameters instead of six.

A)



B)



C)

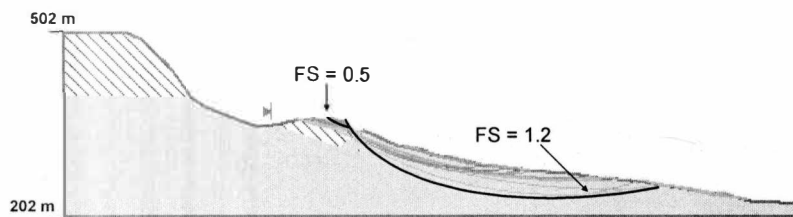


Figure 18. Slip surface prediction results for Mam Tor. A) Predicted versus true slip surface positions for the Mam Tor Landslide. True slip surface positions were determined using boreholes described by Skempton et al., (1989). Predicted slip surfaces were determined using neural network modeling in this study. B) The statistical evaluation of the predicted slip surface location. C) Results of a limit

equilibrium critical surface search using factors of safety between 0.5 and 1.2, indicated by the dark lines.

Predicting Displacements from Meteorological and Groundwater Data using Artificial Neural Networks

Using Ground Water Potentiometric Surface Elevations and Air Temperatures to Predict Displacements

A new ANN model was set up to predict displacement rates from temperature and groundwater elevation data. Ideally elevated ground water results in pore pressure build-up leading to reduced soil shear strength and ultimately displacement. Additionally, studies have documented the seasonal variation of groundwater levels based on freeze/thaw conditions (Chase et al., 2001b, 2007b) in the Lake Michigan coastal bluffs discussed earlier. The objective was to address the following questions:

- Could groundwater and temperature data therefore be used to predict displacements?
- If the first question is answered affirmatively, how far in advance could displacements be predicted when given air temperature and groundwater potentiometric level changes?

Time series graphs of air temperature, potentiometric surface elevations and linear displacement data from a nest of in-place inclinometers at Miami Park South (Well 11 in Figure 11) are displayed in Figure 19. The input parameters were systematically varied to introduce a time lag during neural network training and testing. This was conducted in order to address the second question listed above.

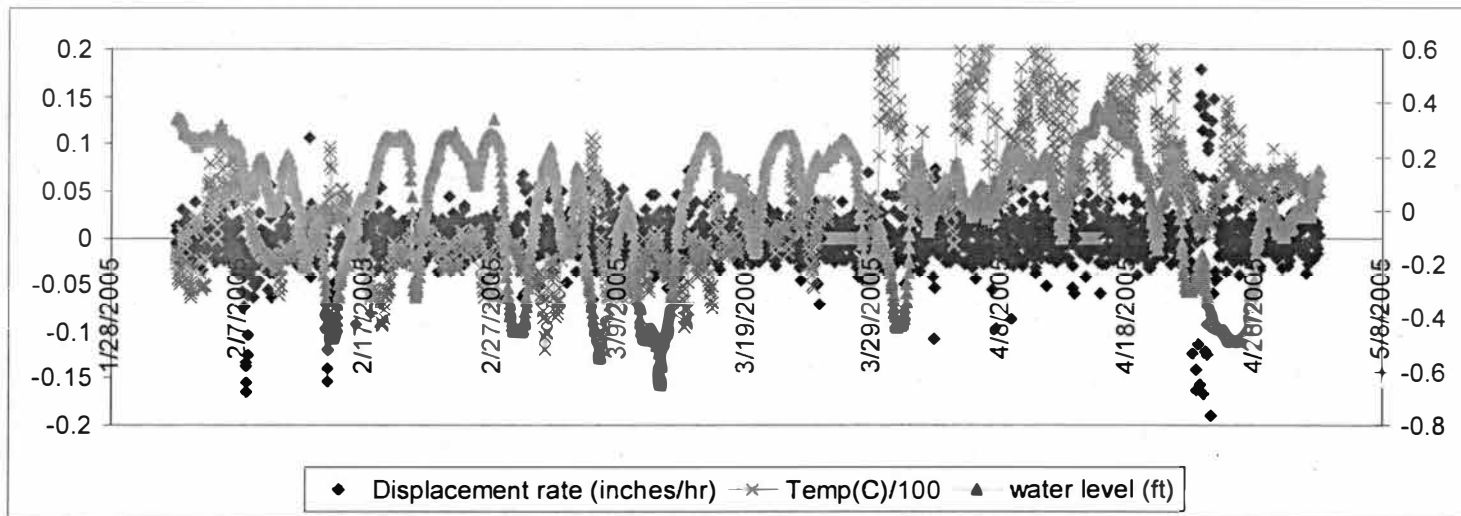


Figure 19. Time series curves showing displacement rates, air temperature and groundwater elevation from well number 11 at the Miami Park South site (Figure 9). Displacement rates are the output variables calculated from inclinometer displacements, while temperature and groundwater elevation are used as inputs during the neural network training and prediction.

Table 8 summarizes the statistics of the modeling results at various time lags expressed in days from one to ten. Pearson correlation coefficient (R) for the test sets range from 0.2 to 0.9. Root mean square (RMS) error values for the test sets range from 0.4 in. (0.01 m) to 5 in. (0.13 m). These values imply that the first objective was met. However these results also imply that the difference between various time lags is too insignificant to be meaningful from a predictive standpoint. In other words, if this ANN was incorporated into a warning system, it would be almost impossible to tell a four-day and a nine-day alarm apart. Therefore more than only two input parameters would be required for the neural network training. A sensitivity analysis, similar to the one conducted above, would have to be executed to determine the significance of each input parameter. Ground water elevations and air temperature input parameters thus provide a starting framework.

Table 8

Summary of statistical modeling results for the neural network displacement rates prediction at various time lags.

one-day time lag							six-day time lag						
X	R	Avg. Abs.	Max. Abs.	RMS	Conf. Interval (95%)	Records	X	R	Avg. Abs.	Max. Abs.	RMS	Conf. Interval (95%)	Records
Train	0.94	0.35	2.05	0.68		1.39 34	Train	0.95	0.19	1.42	0.41		0.82 34
Test	0.90	0.35	1.80	0.61		1.30 15	Test	0.83	0.30	1.56	0.49		1.04 15
two-day time lag							seven-day time lag						
X	R	Avg. Abs.	Max. Abs.	RMS	Conf. Interval (95%)	Records	X	R	Avg. Abs.	Max. Abs.	RMS	Conf. Interval (95%)	Records
Train	0.92	0.31	1.61	0.53		1.07 34	Train	0.35	0.30	2.19	0.63		1.27 34
Test	0.93	0.29	1.41	0.44		0.95 15	Test	0.62	0.32	2.07	0.63		1.36 15
three-day time lag							eight-day time lag						
X	R	Avg. Abs.	Max. Abs.	RMS	Conf. Interval (95%)	Records	X	R	Avg. Abs.	Max. Abs.	RMS	Conf. Interval (95%)	Records
Train	0.87	0.44	4.14	1.01		2.04 34	Train	0.40	0.24	2.03	0.56		1.13 34
Test	0.86	0.46	2.80	0.88		1.89 15	Test	0.33	0.24	2.01	0.53		1.15 15
four-day time lag							nine-day time lag						
X	R	Avg. Abs.	Max. Abs.	RMS	Conf. Interval (95%)	Records	X	R	Avg. Abs.	Max. Abs.	RMS	Conf. Interval (95%)	Records
Train	0.82	0.30	2.03	0.59		1.19 34	Train	0.90	0.12	1.17	0.26		0.54 34
Test	0.44	1.59	18.86	4.95		10.63 15	Test	0.93	0.16	1.30	0.35		0.75 15
five-day time lag							ten-day time lag						
X	R	Avg. Abs.	Max. Abs.	RMS	Conf. Interval (95%)	Records	X	R	Avg. Abs.	Max. Abs.	RMS	Conf. Interval (95%)	Records
Train	0.86	0.38	2.83	0.75		1.52 34	Train	0.88	0.12	0.79	0.22		0.44 34
Test	0.69	0.40	2.25	0.69		1.48 15	Test	0.88	0.15	1.35	0.36		0.77 15

Using Air Temperatures to Predict Groundwater Potentiometric Surface Elevations

The same time series data set from Figure 19 was used to predict water levels from temperature data at different time lags. The objective was to investigate whether air temperatures could be used to predict groundwater elevations, and if so how far in advance. The statistics are summarized in Table 9.

Table 9

Summary of statistical modeling results for the neural network ground water elevation prediction at various time lags.

one-day time lag								six-day time lag							
FT H2O	R	Avg. Abs.	Max. Abs.	RMS	Conf. Interval (95%)	Records		FT H2O	R	Avg. Abs.	Max. Abs.	RMS	Conf. Interval (95%)	Records	
Train	0.77	0.12	0.37	0.16	0.33	31		Train	0.91	0.07	0.31	0.10	0.20	31	
Test	0.29	0.14	0.46	0.20	0.43	14		Test	0.11	0.20	0.51	0.24	0.53	14	
two-day time lag								seven-day time lag							
FT H2O	R	Avg. Abs.	Max. Abs.	RMS	Conf. Interval (95%)	Records		FT H2O	R	Avg. Abs.	Max. Abs.	RMS	Conf. Interval (95%)	Records	
Train	0.50	0.17	0.53	0.23	0.47	31		Train	0.81	0.10	0.39	0.14	0.28	31	
Test	0.33	0.11	0.30	0.15	0.33	14		Test	0.38	0.15	0.72	0.22	0.48	14	
three-day time lag								eight-day time lag							
FT H2O	R	Avg. Abs.	Max. Abs.	RMS	Conf. Interval (95%)	Records		FT H2O	R	Avg. Abs.	Max. Abs.	RMS	Conf. Interval (95%)	Records	
Train	0.45	0.18	0.53	0.23	0.46	31		Train	0.73	0.12	0.49	0.17	0.35	31	
Test	0.44	0.13	0.33	0.15	0.33	14		Test	0.29	0.15	0.55	0.20	0.43	14	
four-day time lag								nine-day time lag							
FT H2O	R	Avg. Abs.	Max. Abs.	RMS	Conf. Interval (95%)	Records		FT H2O	R	Avg. Abs.	Max. Abs.	RMS	Conf. Interval (95%)	Records	
Train	0.74	0.11	0.53	0.17	0.34	31		Train	0.72	0.13	0.52	0.18	0.37	31	
Test	0.50	0.17	0.47	0.21	0.46	14		Test	0.13	0.21	0.52	0.26	0.57	14	
five-day time lag								ten-day time lag							
FT H2O	R	Avg. Abs.	Max. Abs.	RMS	Conf. Interval (95%)	Records		FT H2O	R	Avg. Abs.	Max. Abs.	RMS	Conf. Interval (95%)	Records	
Train	0.81	0.11	0.44	0.15	0.31	31		Train	0.68	0.14	0.46	0.18	0.37	31	
Test	-0.11	0.23	0.59	0.27	0.59	14		Test	0.43	0.17	0.37	0.21	0.46	14	

Pearson correlation coefficients range from 0.1 to 0.5. Root mean square (RMS) errors range from 0.27 ft (0.08 m) to 0.16 ft (0.05 m). In spite of the ability to predict ground water elevations with this level of accuracy, there is still no way of telling results from different time lags apart. Therefore additional input parameters would have to be introduced. A sensitivity analysis, similar to the one conducted above, would have to be executed to determine the significance of each input parameter. Air temperature as an input parameter thus provides only a starting point. Using one input parameter to conduct predictions does not necessarily always lead to

low correlation coefficients as the following example shows.

Example 3: La Mure Landslide Displacements

Description

The Alpine landslide from Example 1 above was studied in greater detail by Nieuwenhuis (1991) who investigated soil moisture conditions in the slide area, shear strength at the slide planes, 3-D slope stability analysis and yearly displacements as related to precipitation, with the goal of simulating the landslide's displacements and stability as a function of time. Using eight years of data, a mathematical model based on plastic flow theory was calibrated to simulate the displacements. Input parameters to the model were the onset of movement, amount and duration of precipitation, and continuation and interruption of displacements. Shear strength reduction due to increased pore pressure conditions was found to be an important factor. However during the summer the landslide could sustain much larger pore pressure increases because of temporary shear strength increases along the slide plane, due to changes in the soil structure during periods without deformation. Factors of safety were found using Janbu's (1968) method to vary generally between 1.05 and 0.98, although their trends or patterns seemed to be more significant than the values themselves in determining displacement. Intermittent movements were also found to be a normal occurrence and down-slope blocks (near the toe) moved with greater velocity than the upslope ones (near the crest). Accumulated blocks and slices at the base of the landslide were believed to slow down the movements. The simulation developed by Nieuwenhuis (1991) could not handle dry spells, because of a reliance on actual "rain days", but was generally acceptable based on how it closely matched measured

displacements.

Artificial Neural Network Model Set Up for La Mure Displacements

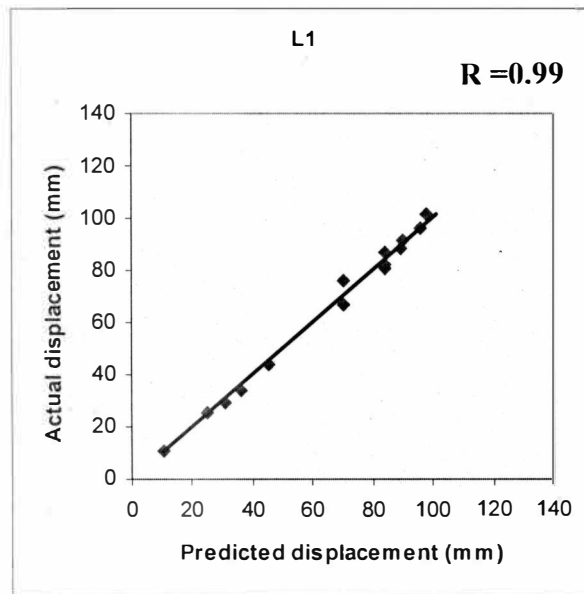
An ANN model was developed using La Mure data and the back propagation algorithm. The goal was to predict field displacements from measured precipitation data. The basis was that precipitation in the region was determined to be a notorious triggering mechanism for slope displacements. Table 10 and Figures 20A - 20B summarize the model results for the training and testing.

Table 10

Summary of neural network displacement modeling results of La Mure Landslide compared with displacements measured by Recorder L1 and L3 (Figure 7)

Results for Site L1						
Statistic	R	Avg. Abs.	Max. Abs.	RMS	Conf. Interval (95%)	Records
Train	0.997073	1.744426	5.509697	2.315643	4.816315	22
Test	0.996388	1.950707	6.121803	2.493152	5.357784	15
Results for Site L3						
Statistic	R	Avg. Abs.	Max. Abs.	RMS	Conf. Interval (95%)	Records
Train	0.997073	1.744426	5.509697	2.315643	4.816315	22
Test	0.996388	1.950707	6.121803	2.493152	5.357784	15

(A)



(B)

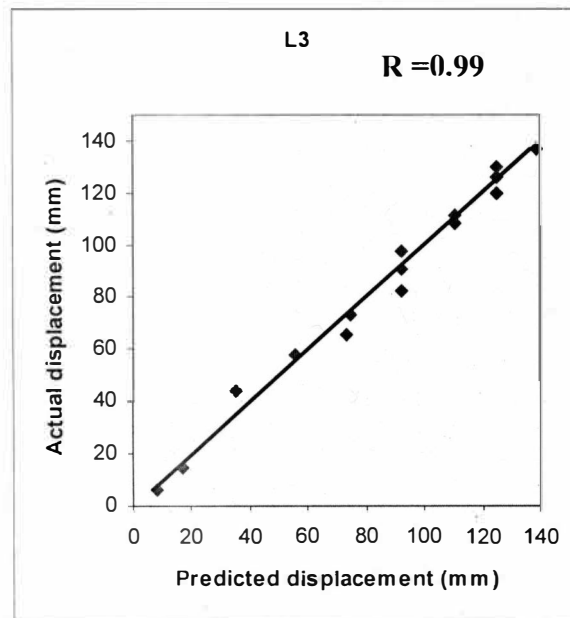


Figure 20. Correlation between displacements predicted by the Artificial Neural Network modeling and displacements measured from the field by recorders: A) L1 and B) L3 in Figure 13 for the La Mure Landslide. Both graphs show a near-ideal straight line fit.

Both survey sites L1 and L3 (Figure 14) show Pearson's correlation

coefficients of 0.99. Figure 21 shows the performance of neural network modeling in predicting displacements in comparison with those recorded at the two survey sites.

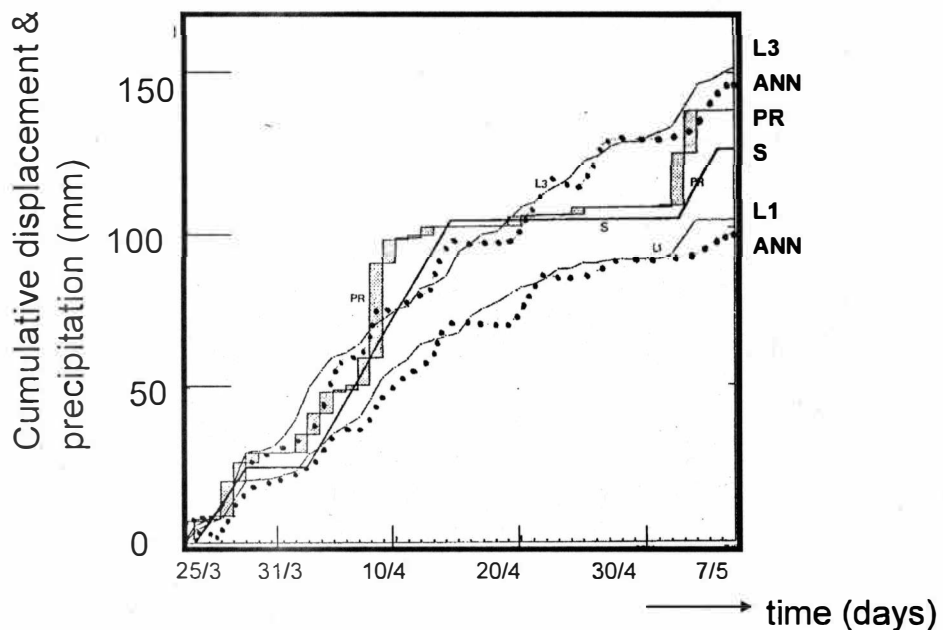


Figure 21. Cumulative displacements and precipitation over time for the La Mure Landslide. L1 and L3 represent displacements measured by two separate recorders (Figure 13), PR represents the cumulative precipitation at the site, s represents the cumulative displacement simulation conducted by Nieuwenhuis (1991) and ANN represents the cumulative displacements predicted by the neural network model discussed in this study

A statistical prediction conducted by Nieuwenhuis (1991) is also shown for comparison. The neural network model fits the true data very well in both cases L1 and L3 with root mean square errors of 2.5 mm and 4.8 mm respectively. In this particular case, using only one input parameter (i.e. precipitation) for the prediction did not result in significantly low correlation coefficients and/or scatter.

Summary and Conclusions

Artificial Neural Network modeling in slope stability studies provides a compelling alternative to other non linear problem solving techniques such as finite elements. Unlike most types of models they require few assumptions pertaining to the data being modeled. Also, their added benefit of being able to adapt to or learn from their environment makes them an invaluable tool in time-variant problems such as creeping landslides or slumps. The first ANN model for this study was developed to predict slip surface positions from displacement data using back propagation and a sigmoid output function. For an active landslide near Lake Michigan, models fit test data well with a root mean square error of about 1.8 m. Sensitivity analysis results show that soil type and cumulative ground elevation change are the most important predictive parameters. The sensitivity results also suggest a stronger rotational component to failure than translation, for the data examined. When this ANN model is applied to two separate landslide studies with similar geology in the French Alps and England, it shows a close match of predicted and measured values, better than a limit equilibrium search with the most conservative criteria. A second ANN model was constructed to predict slope displacement rates from groundwater and air temperature data. This ANN model is able to make a general prediction of displacements. However when a lag time in days is introduced, the difference among the results of models at different time lags is insignificant. Pearson correlation coefficients (R) for the test sets range from 0.2 to 0.9. Root mean square error values for the test sets range from 0.4 in./hr (0.01 m/hr) to 5 in./hr (0.13 m/hr). A third ANN model was developed to predict potentiometric surface elevations from atmospheric temperature at various time lags. This model was also able to make generalized predictions. Pearson correlation coefficients for this model range from 0.1 to 0.5.

Root mean square errors range from 0.27 ft (0.08 m) to 0.16 ft (0.05 m). The input parameters used for training the second and third ANN models in this study provide a foundational framework for warning systems. The fourth ANN model, applied to the French Alps landslide, was developed to predict displacements from precipitation data. The model predicted displacements very well with correlation coefficients of 0.99 and a maximum root mean square error of 4 mm.

Appendix A
Gaussian Quadrature

For nodes (or x values of data) x_0, x_1, \dots, x_n in the interval space $[a, b]$ (See Figure A1 for illustration), the Lagrangean form of the polynomial interpolating the data may be written as:

$$p(x) = \sum_{i=0}^n f(x_i) l_i(x) \quad (1)$$

where

$$l_i(x) = \prod_{\substack{j=0 \\ j \neq i}}^n \frac{x-x_j}{x_i-x_j} \quad (0 \leq i \leq n)$$

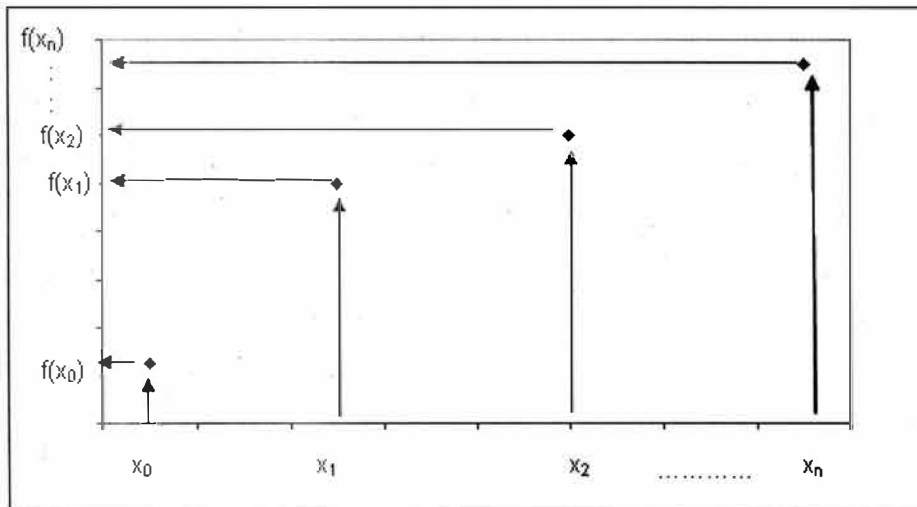


Figure A1. Illustration of discrete data points in a two dimensional $[a, b]$ interval space, where a and b are the endpoints. The values and respective function evaluations at each point, i.e. $x_0, x_1, x_2, \dots, x_n$ are known.

Integrating the polynomial in (1) leads to:

$$\int_a^b p(x)dx = \sum_{i=0}^n (f(x_i) \int_a^b l_i(x)dx) \quad (2)$$

This result in (2) is an approximation of the value of the integration of the actual function $f(x)$ i.e.:

$$\int_a^b f(x)dx \approx \int_a^b p(x)dx \quad (3)$$

A known weight function may be introduced on both sides of Equation (3) to yield the classical Newton-Cotes formulation as follows:

$$\int_a^b f(x)w(x)dx \approx \sum_{i=0}^n (f(x_i) \int_a^b l_i(x)w(x)dx) \approx \sum_{i=0}^n (A_i f(x_i)) \quad (4)$$

If the values of x_i , $f(x_i)$ and A_i are known, a numerical value of the integration of $f(x)$ may be obtained. Essentially one is approximating a series of rectangle areas in an interval and then summing them. If two points are used for the approximation, the result is the trapezoidal rule. If three points are used, the result is Simpson's rule.

A more accurate rule to use is Gaussian quadrature. This approach seeks to obtain the best numerical estimate of an integral by picking optimal abscissas x_i at which to evaluate $f(x)$. By carefully choosing the location of x_i 's and appropriate weighting coefficients, Gaussian quadrature formulas can be achieved whose orders are higher than those of the Newton-Cotes formula. If Equation (4) is expressed as:

$$\int_a^b W(x)f(x)dx \approx \sum_{i=1}^n w_i f(x_i) \quad (5)$$

then a set of weights, w_i and points, $f(x_i)$ can be found to make the approximation exact. These may be obtained by computing the roots of the orthogonal polynomial to the function. A function is said to be orthogonal to another if their scalar product is zero. The roots of the orthogonal polynomial are the abscissas of the Gaussian quadrature formula for the same interval and weighting function. The weights can then be determined by solving a system of linear equations formulated from the orthogonal polynomials of different orders: $i = 0,1,2\dots$. An alternative approach is to obtain the abscissas and weights from available mathematical tables such as Abramowitz and Stegun (1964).

If weight function $W(x) = 1$, then Equation (5) becomes the Gauss-Legendre rule for the integration interval $[-1, 1]$. Any other domain $[a, b]$ must be changed to the interval $[-1, 1]$ before applying Gauss-Legendre rule :

$$\int_a^b f(t)dt = \frac{b-a}{2} \sum_{i=1}^n w_i f\left(\frac{b-a}{2}x_i + \frac{a+b}{2}\right) \quad (6)$$

The rule may be applied for different orders such as $n = 2,3,4,5$ and so on. High order does not necessarily translate to higher accuracy unless the integrand is smooth. For the following Gaussian quadrature rule:

$$\int_a^b f(x)dx = \sum_{i=1}^n w_i f(x_i) + \text{Error_Term} \quad (7)$$

to make the integration exact the error term needs to be made zero. The error term can be made zero for:

$$f(x) = 1, x, x^2, \dots, x^{2n-1} \quad (8)$$

In other words, if $f(x)$ is a polynomial of degree $2n-1$, the Gaussian quadrature of order n becomes exact. The number “ n ” represents the degree of the polynomial whose roots are the abscissas, x_i .

Advantages of Gaussian quadrature include elimination of round off error problems because no subtractions of large numbers occur (unless integrand changes signs in the middle of the domain), and ability to integrate functions with singularities at either bound because values at the limits are not used. For a large interval of integration, the domain can be subdivided into smaller bounds and Gaussian quadrature applied repeatedly using Equation (6) if necessary.

Appendix B
Back Propagation Algorithm

A description of back propagation provided by Poulton (2001), serves as the basis for the discussion that follows. An activation function is one such as a hyperbolic tangent function, sigmoid function, identity function, that may be used to map out a given input. The activation is then multiplied by the connection weights going to the next layer (Figure B1).

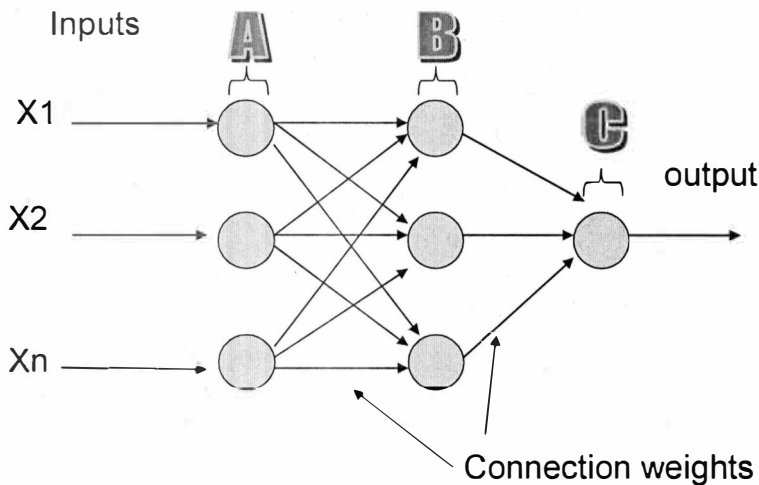


Figure B1. A neural network diagram showing a Multi Layer Perceptron (MLP) or feed forward architecture. X1, X2...Xn represent input parameters. A represents the input layer nodes, B represents the hidden layer nodes and C represents the output node. Each node conducts a mathematical computation on the value it receives and passes it on to the next level via connection weights.

This process is repeated beginning from the input layer all the way to the output layer:

$$Sum_k = \sum_{j=1}^m w_{kj} act_j + w_{kb} \quad (1)$$

$$o_k = f(\text{Sum}_k) \quad (2)$$

where Sum_k = output of a neuron in the output layer (i.e. kth layer), w_{kj} = connection weight between hidden and output layers, act_j = activation of the output of a neuron in the hidden (i.e. jth layer), w_{kb} = the bias weight, o_k = activation of neuron in the output layer

After the first iteration the calculated output will differ from the desired one in the training file. The mean squared error, e_p , can be calculated as:

$$e_p = \frac{1}{2} \sum_{k=1}^L (d_{pk} - o_{pk})^2 \quad (3)$$

where d_{pk} = desired output and o_{pk} = calculated output

The goal of neural network training is to minimize the error with respect to the connection weights, so there is need to minimize the partial derivative.

$$\frac{\partial e_p}{\partial w_{kj}} = \frac{\partial e_p}{\partial \text{Sum}_{pk}} \frac{\partial \text{Sum}_{pk}}{\partial w_{kj}} \quad (4)$$

Equation (4) can be solved by looking at each component individually

$$\frac{\partial \text{Sum}_{pk}}{\partial w_{kj}} = \frac{\partial}{\partial w_{kj}} \sum_k w_{kj} \text{act}_{pji} = \text{act}_{pj} \quad (5)$$

If we let

$$\delta_{pk} = \frac{\partial e_p}{\partial \text{Sum}_{pk}} \quad (6)$$

and it follows that

$$\frac{\partial e_p}{\partial w_{kj}} = \delta_{pk} \text{act}_{pj} \quad (7)$$

Rewriting Equation 6 gives

$$\frac{\partial e_p}{\partial \text{Sum}_{pk}} = \frac{\partial e_p}{\partial \omega_{pk}} \frac{\partial \omega_{pk}}{\partial \text{Sum}_{pk}} \quad (8)$$

Each component from (8) can be solved as:

$$\frac{\partial \omega_{pk}}{\partial \text{Sum}_{pk}} = f'_k(\text{Sum}_{pk}) \quad (9)$$

and

$$\frac{\partial e_p}{\partial o_{pk}} = (d_{pk} - o_{pk}) \quad (10)$$

Substituting (9) and (10) into (8) gives us

$$\delta_{pk} = (d_{pk} - o_{pk}) f'_k (Sum_{pk}) \quad (11)$$

Substituting (11) into (7) gives us the weight changes required for the connections between the hidden and output layer:

$$\Delta w_{kj} = \frac{\partial e_p}{\partial w_{kj}} = (d_{pk} - o_{pk}) f'_k (Sum_{pk}) act_{pj} \quad (12)$$

The next procedure is to find the weight changes required for the connections between the input and hidden layers. The relationship between the calculated values for each output neuron and the activation of the neurons in the hidden layer can be expressed as:

$$\frac{\partial e_p}{\partial w_{ji}} = \frac{1}{2} \sum_k \frac{\partial}{\partial w_{ji}} (d_{pk} - o_{pk})^2 \quad (13)$$

Expanding this gives

$$\frac{\partial e_p}{\partial w_{ji}} = \sum_k (d_{pk} - o_{pk}) \frac{\partial w_{pk}}{\partial \text{Sum}_{pk}} \frac{\partial \text{Sum}_{pk}}{\partial \text{act}_{pj}} \frac{\partial \text{act}_{pj}}{\partial \text{Sum}_{pj}} \frac{\partial \text{Sum}_{pj}}{\partial w_{ji}} \quad (14)$$

Solving for each component in (14):

$$\frac{\partial w_{pk}}{\partial \text{Sum}_{pk}} = f'_k(\text{Sum}_{pk}) \quad (15)$$

$$\frac{\partial \text{Sum}_{pk}}{\partial \text{act}_{pj}} = \frac{\partial (\sum w_{kj} (f(\sum w_{ji} x_{pi})))}{\partial (f(\sum w_{ji} x_{pi}))} = w_{kj} \quad (16)$$

$$\frac{\partial \text{act}_{pj}}{\partial \text{Sum}_{pj}} = f'_j(\text{Sum}_{pj}) \quad (17)$$

$$\frac{\partial \text{Sum}_{pj}}{\partial w_{ji}} = \frac{\partial (\sum w_{ji} x_{pi})}{\partial w_{ji}} = x_{pi} \quad (18)$$

Substituting these components back into (14) gives:

$$\frac{\partial e_p}{\partial w_{ji}} = \sum_k (d_{pk} - o_{pk}) f'_k(\text{Sum}_{pk}) w_{kj} f'_j(\text{Sum}_{pj}) x_{pi} \quad (19)$$

Based on Equation (11), Equation (19) can be simplified as:

$$\frac{\partial e_p}{\partial w_{ji}} = (f'_k(\text{Sum}_{pj}) \sum \delta_{pk} w_{kj}) x_{pi} \quad (20)$$

The weight changes on the connections between the hidden and input layers can then be expressed as:

$$\Delta w_{ji} = \frac{\partial e_p}{\partial w_{ji}} = \delta_{pj} x_{pi} \quad (21)$$

where $\delta_{pj} = f'_j(\text{Sum}_{pj}) \sum_k \delta_{pk} w_{kj}$

A way is needed to change the weights in proportion (η) to the error. Using the delta rule the new weights between the input and hidden layers become:

$$w_{ji}^{new} = w_{ji}^{old} + \eta \delta_{pj} x_{pi} \quad (22)$$

The new connection weights between the hidden and output layers become

$$w_{kj}^{new} = w_{kj}^{old} + \eta \delta_{pk} act_{pj} \quad (23)$$

After the weights are changed, the inputs are reapplied and the whole process repeated. This is what is known as back propagation learning, which represents a gradient descent technique.

BIBLIOGRAPHY

- Abramowitz, M., and Stegun, I.A., 1964, Handbook of Mathematical Functions with Formulas, Graphs and Mathematical Tables, National Bureau of Standards (NBS), Washington DC.
- Allmendinger, R. W., 1998, Inverse and Forward numerical modeling of trishear fault-propagation folds: *Tectonics*, 17(4), 640-656.
- Arndt, C., Fecso, B., Preckel, P.V., Stoneman, B., 2001, Soil selection for use in environmental analysis, *Journal of Soil and Water Conservation* 56(2), 165-171
- Baker, R. and Leshchinsky D, 2001, Spatial distribution of safety factors, *Journal of Geotechnical and Geoenvironmental Engineering*, 127(2), 135-145.
- Cao, J., 2002, *Neural Network Modeling and Analytical Modeling of Slope Stability*: Unpublished PhD Dissertation, Department of Civil Engineering, University of Oklahoma, Norman, Oklahoma, 129 p.
- Chase, R.B., Chase, K.E., Kehew, A.E., and Montgomery, W. W., 2001a, Determining the kinematics of slope movements using low-cost monitoring and cross-section balancing: *Environmental & Engineering Geoscience*, 7(2), 193-203.
- Chase, R.B., Kehew, A.E., and Montgomery, W.W., 2001b, Determination of Slope Displacement mechanisms and Causes Using New geometric Modeling Techniques and Climate Data. In Harmon, R.S. and Doe III, W. W. (Editors), *Landscape Erosion and Evolution Modeling*: Kluwer Academic Publishers, New York, pp.57-87.
- Chase, R.B., Kehew, A.E., Glynn, M.E., and Selegean, J.P., 2007a, Modeling debris slide geometry with balanced cross-sections: a rigorous field test: *Environmental & Engineering Geoscience*, 13(1), 193-203.
- Chase, R.B., Kehew, A.E., Kaunda R.B., and Glynn, M.E., 2007b, Mitigation of slope failures in freeze/thaw environment by removal of ground water, Proceedings of the First North American Landslide, Vail, CO.
- Chen, W.F., 1975, *Limit Analysis and Soil Plasticity*, Elsevier, Amsterdam, 638 p.

- Chen J., Yin J.-H., Lee C.F., 2004, Rigid finite element method for upper bound limit analysis of soil slopes subjected to pore water pressure, *Journal of Engineering Mechanics* 130(8), 886-893.
- Chowdhury, R.N., 1978, Propagation of failure surfaces in natural slopes: *Journal of Geophysical Research*, 83, 5983-5988.
- Cooper, M.R., Bromhead, E.N., Petley, D.J., and Grant, D.I., 1998, The Selborne cutting stability experiment, *Geotechnique*, 48, 83-101.
- Coppola, E.A., Rana, A.J., Poulton, M.M., Szidarovsky F., and Uhl, V.W., 2005, A neural network model for predicting aquifer water level elevations, *Ground Water*, 43(2), 231-241.
- Dahlstrom, C.D.A., 1969, Balanced cross sections: *Canadian Journal of Earth Science*, 6, 743-7575.
- Duncan, J.M., 1996a, State of the art: limit equilibrium and finite element analysis of slopes, *Journal of Geotechnical Engineering*, 122(7), 577-596.
- Duncan, J.M., 1996b, Soil slope stability analysis: p.337-271 in Turner, A.K., and Schuster, R.L., (eds.), *Landslides: Investigation and Mitigation: Transportation Research Board Special Report 247*, 675 p.
- Ellis, G.W., Yao, C., Zhao, R., Penumadu, D., 1995, Stress-strain modeling of sand using Artificial Neural Networks, *Journal of Geotechnical Engineering*, 121(5), 429-435.
- Erslev, E.A., 1991, Trishear fault-propagation folding, *Geology* 19, 617-620.
- Finch, E., Hardy, S., Gawthorpe, R., 2003, Discrete element modeling of contractional fault propagation folding above rigid basement blocks, *Journal of Structural Geology*, 25, 515-528.
- Ghaboussi, J., and Sidarta, D.E., 1998, New nested adaptive neural networks for constitutive modeling, *Computers and Geotechnics*, 22(1), 29-52.
- Griffiths, D.V. and Lane, P.A., 1999, Slope stability analysis by finite elements, *Geotechnique*, 49 (3), 387- 403.
- Griffiths, D.V. and Fenton, G.A., 2004, Probabilistic slope stability analysis by finite elements., *Journal of Geotechnical and Geoenvironmental Engineering* 130(5), 507-518.
- Habibagahi, G., and Bamdad, A. 2003., A neural network framework for mechanical behavior of unsaturated soils, *Canadian Geotechnical Journal*, 40, 684-693.

- Hampton, M.A., Griggs, G.B., Edil, T.B., Guy, D.E., Kelley, J.T., Komar, P.D., Mickelson, D.M., and Shipman, H.M., 2004, *Processes that govern the formation and evolution of coastal cliffs*, in Hampton, M.A. and Griggs, G.B., (eds.) *Formation, Evolution, and Stability of Coastal Cliffs: Status and Trends*: U.S.G.S. Professional Paper 1693, p. 7-38.
- Hardy, S., and Ford, M., 1997, Numerical modelling of trishear fault-propagation folding and associated growth strata: *Tectonics*, 16(5), 841-854.
- Horton, R.E., 1938, Phenomena of the Contact Zone between the ground surface and a layer of melting snow, *Bulletin No. 23, Association Internationale d'Hydrologie Scientifique*, Paris, 545-561.
- Hwang, C., Wang, C.G., and Hsiao, Y.S., 2003, Terrain correction computation using a Gaussian quadrature: *Computers and Geosciences* 29(10), 1259-1268.
- Janbu, N., 1968, Slope Stability Computations, *Soil Mechanics and Foundation Engineering Report*, Technical University of Norway, Trondheim
- Johnson, K.A., and Sitar, N., 1990, Hydrologic conditions leading to debris-flow initiation, *Canadian Geotechnical Journal*, 27, 789-801.
- Juang, C.H., Jiang, T., and Christopher R.A. 2001, Three-dimensional site characterization: neural network approach., *Geotechnique*, 51(9), 799-809.
- Kamai, T., 1998, Monitoring the process of ground failure in repeated landslides and associated stability assessments: *Engineering Geology*, 50, 71-84.
- Kim J.Y. and Lee S.R., 1997, An improved search strategy for the critical slip surface using finite element stress fields, *Computers and Geotechnics*, 21(4), 295-313.
- Kincaid, D., and Cheney, W., 2002, *Numerical Analysis: Mathematics of scientific computing*, Third Edition: BROOKS/COLE, Pacific Grove, CA, 788 p.
- Lambe, T.W., and Whitman, R.V., 1969, *Soil Mechanics*, John Wiley & Sons, New York, 553p.
- Liu, Y., Guo, H.C., Zou, R. and Wang, L.J., 2006, Neural network modeling for regional hazard assessment of debris flow in Lake Qionghai Watershed, China. *Environmental Geology* 49, 968-976.
- Mathewson, C.C., Keaton, J.R., and Santi, P.M., 1990, Role of bedrock groundwater in the initiation of debris flows and sustained post storm stream discharge, *Bulletin of the Association of Engineering Geologists*, 27(1), 73-78.

- Montgomery, William.W., 1998, *Groundwater Hydraulics and Slope Stability Analysis: Elements for prediction of shoreline Recession*: Unpublished Ph.D. Dissertation, Department of Geosciences, Western Michigan University, 256 p.
- Neaupane, K. and Achet, S., 2004, Some applications of a back propagation neural network in geo-engineering, *Environmental Geology*, 45, 567-577.
- Nieuwenhuis, J.D., 1991, *The Lifetime of A Landslide: Investigations in the French Alps*, A.A. Balkema, Rotterdam, The Netherlands, 144 p.
- Parker, D.B., 1985, *Learning Logic*, Technical Report TR-47, Center for Computational Research in Economics and Management Science, Massachusetts Institute of Technology, Cambridge, MA.
- Petley D.N., Carey J., Higuchi T., Petley D.J., and Bulmer M.H., 2005, Development of progressive landslide failure in cohesive materials: *Geology* 33(3), 201-204.
- Poulton, M., 2001, *Computational neural networks for Geophysical Data Processing*, Paragons Press Ltd, Amsterdam, The Netherlands, 335 p.
- Reid, M.E., Nielsen, H.P., and Dreiss, S.J., 1988, Hydrologic factors triggering a shallow hillside failure, *Bulletin of the Association of Engineering Geologists*, 25(3), 349-361.
- Rumelhart, D.E., Hinton, G.E., and Williams, R.J., 1986, Learning internal representations by error propagation: in D.E. Rumelhart and J.L. McClelland, eds., *Parallel distributed processing* Vol 1, p 318-362. Cambridge, MA: MIT Press, 550 p.
- Rutter, E.H., Arkwright J.C., Holloway, R.F. and Waghorn, D., 2003, Strains and displacements in the Mam Tor landslip, Derbyshire, England, *Journal of the Geological Society*, 160, 735-744.
- Schuster, R.L., 1996, Socioeconomic significance of landslides: p. 12-35 in Turner, A., K. and Schuster, R.L., (eds.) *Landslides: Investigation and Mitigation*, Special Report 247, Transportation Research Board, 675p.
- Side, R.C., 1984, Shallow groundwater fluctuations in unstable hillslopes of coastal Alaska, *Zeitschrift für Gletscherkunde und Glazialgeologie*, 20, 79-95.
- Simon, A., Larsen, M.C., Hupp, C.R., 1990, The role of soil processes in determining mechanisms of slope failure and hillside development in a humid tropical forest Eastern Puerto Rico, *Geomorphology*, 3, 263-286.

- Skempton, A.W., Leadbeater, A.D, and Chandler, R.J., 1989, The Mam Tor landslide, North Debyshire, *Philosophical Transactions of the Royal Society of London*, Series A, 329, 503-547.
- Srbulov M., 1997, On the influence of soil strength brittleness and nonlinearity on slope stability, *Computer and Geotechnics*, 20 (1), 95-104.
- Stark, T.D., Choi, H., and McConne S., 2005, Drained shear strength parameters for analysis of landslides, *Journal of Geotechnical and Geoenvironmental Engineering* 131(5), 575-588.
- Suemine, A. 1983, Study on landslide mechanism in the area of crystalline schist (part 1)—an example of propagation of Rankine state, *Bulletin of the Disaster Prevention Research institute of Kyoto University*, 33(3), 105-127.
- Suppe, J., and Medwedeff, D., 1990, Geometry and kinematics of fault-propagation folding: *Eclogae Geologicae Helvetiae*, 83, 409-454.
- Terzaghi, K. and Peck, R.B., 1948, *Soil Mechanics in Engineering Practice*, Wiley, New York, 91p.
- Van Genuchten, P.M.B., Nieuwenhuis J.D., 1990, On the Stability of Seasonally Sliding Soil Masses in the French Alps, *Engineering Geology*, 28, 41-69.
- Varnes, D.J., 1978, Slope movement Types and Processes, In Special Report 176: Landslides: Analysis and Control (R.L. Schuster and R.J. Krizek, eds), TRB, National Research Council, Washington DC.
- Waltham, D., 1992, Mathematical modeling of sedimentary basin processes, *Marine and Petroleum Geology*, 9, 265-273.
- Wang, H.B., Xu, W.H., and Xu, R.C., 2005, Slope stability evaluation using back propagation neural networks, *Engineering Geology*, 80, 302-315.
- Werbos, P.J., 1974, Beyond Regression: *New Tools for Prediction and Analysis in the Behavioral Sciences*: Unpublished Ph.D. Dissertation, Department of Applied Mathematics, Harvard University.
- Wieczorek, G.F., 1996, Landslide triggering mechanisms: p. 76-90 in Turner, A., K. and Schuster, R.L., (eds.) *Landslides: Investigation and Mitigation*, Special Report 247, Transportation Research Board, 675p.
- Wilson, R.C., 1989, *Rainstorms, pore pressures, and debris flows: A theoretical framework*, in Sadler, P. and Morton, D.M. (eds.), *Landslides in a Semi Arid Environment*, Inland Geological Society, Riverside, California, Vo.2, p.101-117.

- Wilson, C.J., and Dietrich, W.E., 1987, *The contribution of bedrock groundwater flow to storm runoff and high pore pressure development in hollows*, in *Erosion and Sedimentation in the Pacific Rim*, International Association of Hydrological Sciences, Delft Netherlands, Publication 165, p. 49-59.
- Woodward, N.B.; Boyer, S.E.; and Suppe, J., 1985, *An Outline of Balanced Cross-Sections*: University of Tennessee Publication, Knoxville, TN, 176p.
- Yang, X.L. and Yin, J.H., 2004, Slope stability analysis with nonlinear failure criterion, *Journal of Engineering Mechanics*, 130(3), 267-273.
- Yeh, H.D., Yang, S. Y., and Peng H. Y., 2003, A new closed-form solution for a radial two-layer drawdown equation for groundwater under constant-flux pumping in a finite-radius well: *Advances in Water Resources* 26(7), 747-757.
- Zhu, J., Zaman, M. M., and Anderson, S.A., 1998, Modeling of soil behavior with a recurrent neural network, *Canadian Geotechnical Journal*, 35(5), 858-872.